scientific reports

OPEN

Computational supported experimental insights in adsorption of Congo Red using ZnO/doped ZnO in aqueous solution

Ayushi Prajapat[1,2,7], Mohd. Aslam[1,3,7], Ishika Rana[1,4,7], Kumar Rakesh Ranjan[4], Prashant Singh[1✉], Chandrabhan Verma[6], Akram AlFantazi[6✉] & Kamlesh Kumari[5✉]

The rapid growth of industrialisation has led to the discharge of harmful effluents into water bodies, severely disrupting the balance of ecosystems. The detection and removal of dyes from wastewater remains a significant challenge. In this study, we report the synthesis of zinc oxide (ZnO) and its doped derivatives through a facile chemical method, followed by comprehensive characterisation and analysis to assess their potential in various applications. The structural properties of the synthesised materials were confirmed by X-ray diffraction (XRD), which verified their crystalline nature and phase purity. Morphological analysis using field emission scanning electron microscopy (FE-SEM) coupled with energy dispersive X-ray analysis (EDAX) revealed well-defined nanostructures and uniform elemental distribution. The adsorption ability of the synthesized adsorbents was investigated through electrochemical methods, cyclic voltammetry and Tafel plots, which demonstrated enhanced conductivity and charge transfer characteristics. Additionally, theoretical studies through molecular modelling and molecular dynamic simulations were employed to elucidate the interactions between Congo red molecules and the surface of the synthesized compounds. Adsorption experiments were conducted to evaluate the efficacy of ZnO and its doped variants as adsorbents. To investigate any structural or functional changes after dye adsorption FTIR and XRD were compared, provided a deeper insight into the adsorption mechanism. This multi-faceted approach highlights the potential of ZnO-based materials for effective wastewater treatment and other environmental applications.

Keywords ZnO & doped ZnO, MD simulations, Cyclic voltammetry, Adsorption studies

Dyes have revolutionized various industries, extending their application from textiles industries to food, plastics, cosmetics, leather, and even solar cells. However, the extensive utilization of these dyes is potentially hazardous to human health and the environment due to their toxic, carcinogenic, and non-biodegradable nature[1,2]. The azo dyes in particular are most widely used due to their extensive applications; the difficulty in their degradation and high toxicity makes their removal from wastewater a matter of concern[3]. Congo red (CR) dye, a representative of azo dyes is an organic pollutant known for its applicability in printing, rubber and dying industries is potentially toxic due to its persistence in wastewater thus leading to unintended biomagnification[4,5]. Conventional methods for the sensing of dyes require sophisticated instrumentations and are often time-consuming[6]. Therefore, the need for the development of cost-effective, rapid and sensitive sensing technologies is gaining the attention of researchers. The adsorption technique for the removal of dyes is one of the oldest wastewater treatments yet most effective due to its simplistic mechanism, low cost and reusability[7,8].

Metal oxide, modified metal oxides, metal-organic framework (MOF), carbon nanotubes, etc. nanomaterials are considered excellent for adsorption due to their enhanced surface area, high absorbance and, easy synthesis[9–12]. Adsorbents like metal oxides have advantages such as eco-friendliness, abundant natural deposits,

[1]Department of Chemistry, Atma Ram Sanatan Dharma College, University of Delhi, New Delhi, India. [2]Department of Chemistry, University of Delhi, Delhi, India. [3]Department of Chemistry, SRM Institute of Science & Technology, Delhi-NCR Campus, Modinagar, Ghaziabad, UP, India. [4]Department of Chemistry, Amity Institute of Applied Sciences, Amity University, Noida, India. [5]Department of Zoology, University of Delhi, Delhi, India. [6]Department of Chemical Engineering, Khalifa University of Science and Technology, P.O. Box 127788, Abu Dhabi, United Arab Emirates. [7]These authors contributed equally: Ayushi Prajapat, Mohd. Aslam and Ishika Rana. ✉email: psingh@arsd.du.ac.in; akram.alfantazi@ku.ac.ae; kkumari@zoology.du.ac.in

and low cost but due to their oversized dimensions, they have limited adsorption capacity and rate[13]. Among metal oxide-based adsorbents, Zinc oxide (ZnO) and its composites have been extensively used for various applications owing to their versatile properties such as optical, catalytic, electrical, UV-absorbing, photocatalytic properties as well as its lower cost. Various composites of ZnO have been used for the removal of CR from wastewater[14–16].

Radwan et al., 2024, have reported adsorption of CR by synthesized ZnO, CuO, and biosynthesized nanocomposite ZnO/CuO (BZC), where the BZC nanocomposite showed a high removal capacity of 90.14 mg g^{-1}. The mechanism of the adsorption is accredited to the electron transfer reaction occurring between the dye and the nanocomposite; as the pH decreases the positive surface charge of the BZC increases, facilitating the electron transfer to the BZC from the anionic dye[17]. Karamipour et al., 2016, have studied the adsorption of CR by the ZnO-ZnFe$_2$O$_4$-polypyrrole magnetic nanocomposite. The synthesized nanocomposite was characterized by XRD, FT-IR, SEM and UV-Vis. The results showed that the composite possesses higher adsorption capacity than pure ZnO and ZnO-PPy. The pH-based adsorption study indicated higher adsorption of the dye in an acidic medium of up to 98% [18]. The removal of CR by doped ZnO nanoparticles has also been studied by Singh et al., 2023, where they doped the ZnO with three transition metals Fe, Co, and Mn. The Fe-doped ZnO showed the minimum CR removal capacity due to their agglomeration. However, the maximum CR removal capacity of Co-doped ZnO was reported as high as 230 mg g^{-1}[19]. Additionally, the removal of CR by ZnO and ZnO/Al$_2$O$_3$ composite has been studied by Mo et al., 2022, It showed the maximum adsorption capacity of 24.57 mg g^{-1} at 250 mg/L CR dye[20].

The insights into the adsorption process or the underlying mechanism of the dye adsorption on the surface of the adsorbent can be investigated by model fitting, density functional theory calculation (DFT), characterization analysis, statistical physics theory calculation, etc[21]. Rahali et al., 2021, synthesized the Ba-doped ZnO by co-precipitation method and studied the adsorption capacity of CR onto the nanocomposite via DFT computations. The nanocomposite demonstrated the maximum adsorption capacity of 1614.26 mg/g, proving its utility to eliminate CR from wastewater[22]. Das et al., 2023, doped Mn into ZnO to enhance the optical properties of the synthesized compound making it an efficient photoactive material for CR degradation and wastewater treatment. Herein, the effect of Mn doping on the ZnO was investigated theoretically via DFT calculations. The DFT result shows that the photogenerated holes are trapped by the vacant oxygen promoting carrier recombination. However, due to the presence of the Mn dopant, the electronic structure of these vacancies modifies in a favourable way[23].

This paper presents a comparative study of the adsorption capacity of ZnO with various synthesized doped ZnO materials. The adsorption capacity of these adsorbents has been analyzed by various studies, namely, electrochemical, computational and experimental to ensure correlation in the results to achieve a method to predict the adsorption capacity of various adsorbents beforehand performing the experimental studies. The synthesis and characterization of ZnO and its doped compounds with Co, La and Ce as dopants for the effective sensing of CR dye. The choice of specific dopants was motivated by the performance of Co-doped ZnO in the study conducted by Singh et al.[19]. and the low availability of literature available on Lanthanide-doped ZnO for this application. The particular Lanthanides have been chosen as per the ease of availability. The structural, compositional and morphological properties of the synthesized compounds were comprehensively investigated using various characterization techniques. The adsorption performance of the synthesized adsorbents was compared from various studies, i.e. experimental, electrochemical and computational methods. The electrochemical performance was assessed using cyclic voltammetry (CV) and tafel plot in the presence of CR. Additionally, molecular modelling and molecular dynamic simulations were employed to understand the interaction of CR molecules to the surface of synthesized compounds.

Experimental section
Chemicals and reagents
The chemicals employed were of good quality, chosen for their analytical grade and heightened purity. Zinc nitrate hexahydrate (Zn (NO$_3$)$_2$·6H$_2$O, AR grade, 99.0% purity) from Central Drug House (P) Ltd. India, sodium hydroxide (NaOH, LR grade, 99.0% purity) from MOLYCHEM India. cobalt sulphate (II) heptahydrate (CoSO$_4$0.7 H$_2$O) (extra pure grade, 97.0% purity) from Loba Chemie Pvt. Ltd. India, lanthanum (III) nitrate hexahydrate (La (NO$_3$)$_3$.6H$_2$O, AR grade, 99.0% purity) ceric (IV) sulphate pentahydrate (Ce(SO$_4$)$_2$. 4H$_2$O, AR grade, 99.5% purity), from SRL Chemicals India, CR and ethanol.

Synthesis of ZnO nanoparticles
To prepare ZnO, the sol-gel method was employed, and the concentration of the dopant salts was chosen based on a thorough review of reported literature[24,25]. Initially, two beakers containing 100 mL of deionized water (DI water) each were taken and marked as A and B. Then, 2.98 g of Zn (NO$_3$)$_2$·6 H$_2$O was added in beaker A and 0.8 g of NaOH in beaker B. The solutions were stirred for about 5 min to get a homogenous solution. The solution B was added to A with constant stirring at 60 °C in 1 h. The solution was stirred for 3 h and then centrifuged to collect the gel residue. Finally, the gel residue at the bottom of the centrifuge tube was collected for drying. The gel once dried, the obtained product was placed in the muffle furnace at 500 °C temperature for 2 h (Fig. 1).

Synthesis of doped ZnO compounds
Co-doped ZnO was synthesized by first dissolving 2.98 g of Zn(NO$_3$)$_2$·6H$_2$O in 100 mL of deionized water, followed by stirring. To this solution, 0.1 M of Co dopant (CoSO$_4$·7 H$_2$O) was added. In a separate beaker, 0.8 g of NaOH was dissolved in 100 mL of deionized water. The NaOH solution was then gradually added to the Zn(NO$_3$)$_2$·6H$_2$O and CoSO$_4$·7 H$_2$O mixture, with continuous stirring at 50–60 °C for 1 h. The resulting solution was stirred for an additional 3 h before being centrifuged, with the final product collected into a petri dish. This
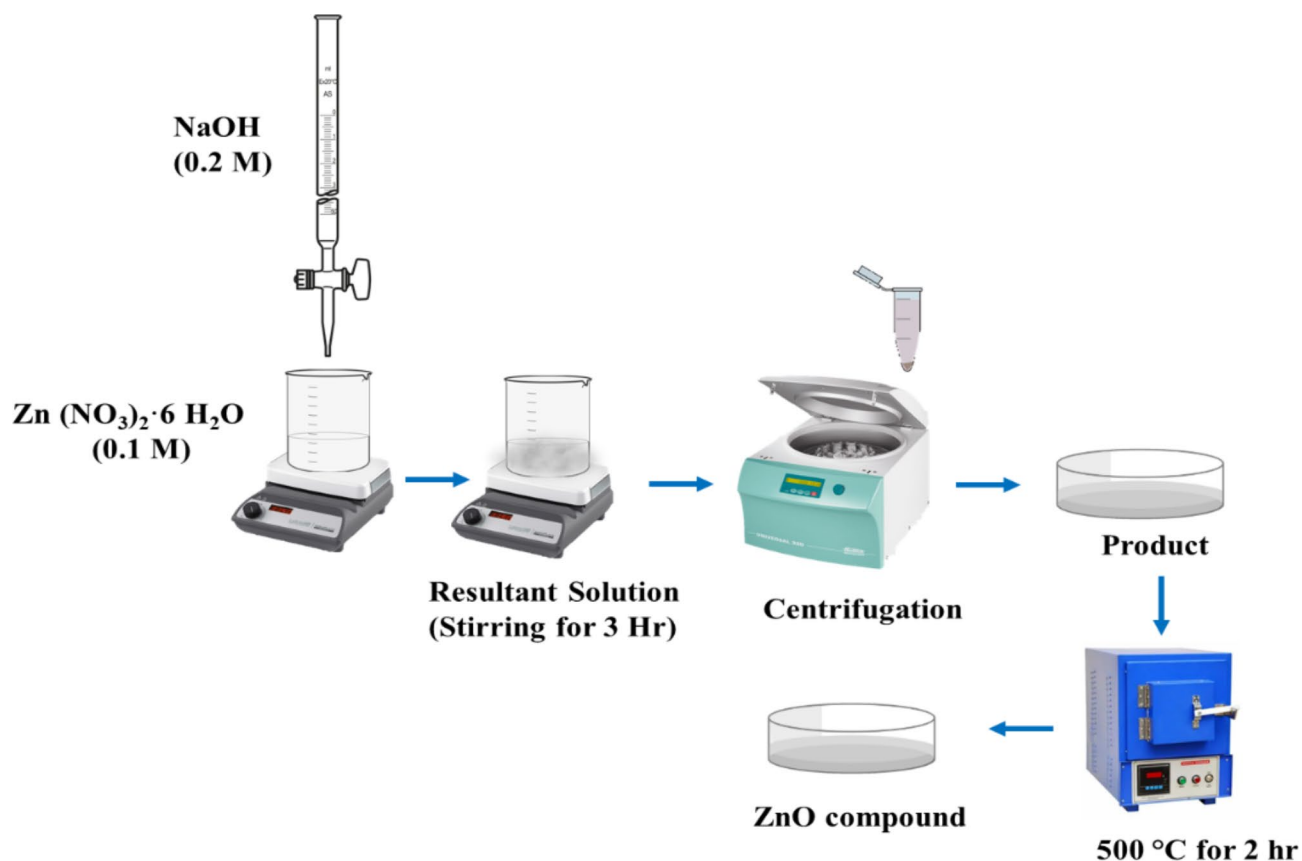
Fig. 1. Systematic representation of synthesis procedure of ZnO.

product was then dried and heated in a muffle furnace at 500 °C for 2 h. The same procedure was followed to prepare other doped ZnO compounds i.e., La-doped ZnO using $La(NO_3)_3 \cdot 6H_2O$ as the La dopant, and Ce-doped ZnO using $Ce(SO_4)_2 \cdot 4H_2O$ as the Ce dopant.

Characterization techniques
Powder XRD analysis of synthesized samples was performed in a Miniflex 600 Rigaku, to check the crystal structure of the prepared samples. The surface morphologies of the synthesized compounds were examined by FE-SEM using Zeiss, Sigma 300. The EDAX and elemental mapping analysis were performed to examine the chemical compositions and purity of the samples.

Electrochemical studies
The electrochemical studies (Cyclic voltammetry and Tafel), were performed with CH Instruments 604E electrochemical analyzer. The system was a three-electrode system with a glassy carbon electrode (GCE) as the working electrode, 3.0 M KCl-filled Ag/AgCl as the reference electrode, and Platinum wire as the counter electrode (Fig. 2). The CV was done from a potential range of -1.4 V to + 1.0 V with a sensitivity of the system set at 1×10^{-4}. Potassium chloride (KCl) was used as the electrolyte. For scan rate CV analysis, the scan rate taken was 50 mV/s, 100 mV/s, 200 mV/s, 300 mV/s, and 400 mV/s. For Tafel plot the potential range was similar to CV which is -1.4 V to + 1.0 V.

Preparation of modified electrode
The suspension for ZnO and its doped materials (Co-doped ZnO, La-doped ZnO, and Ce-doped ZnO) were prepared in acetone (0.01 g in 5 mL). The GCE electrode was polished with alumina powder and rinsed with distilled water. Then 5 μL suspension of aforementioned materials were drop-casted on the GCE for sensing studies. The electrode was left to dry for 30 min and then used for CV and tafel plot.

Computational details
Simulation cell construction
The simulation cell of ZnO and the doped ZnO (Co-doped ZnO, La-doped ZnO and Ce-doped ZnO) were prepared by taking the (1 0 0) plane surface of the ZnO unit cell, of thickness 3.333 Å. To obtain the supercell formation, an almost square surface was produced with u/v being 8/5, and a vacuum slab of thickness 20 Å along the position (1 0 0) in the z direction was placed. For doped ZnO, 4 atoms along each edge centre of the ZnO supercell top surface were doped with the respective metals i.e., Co, La and Ce. For all the calculations
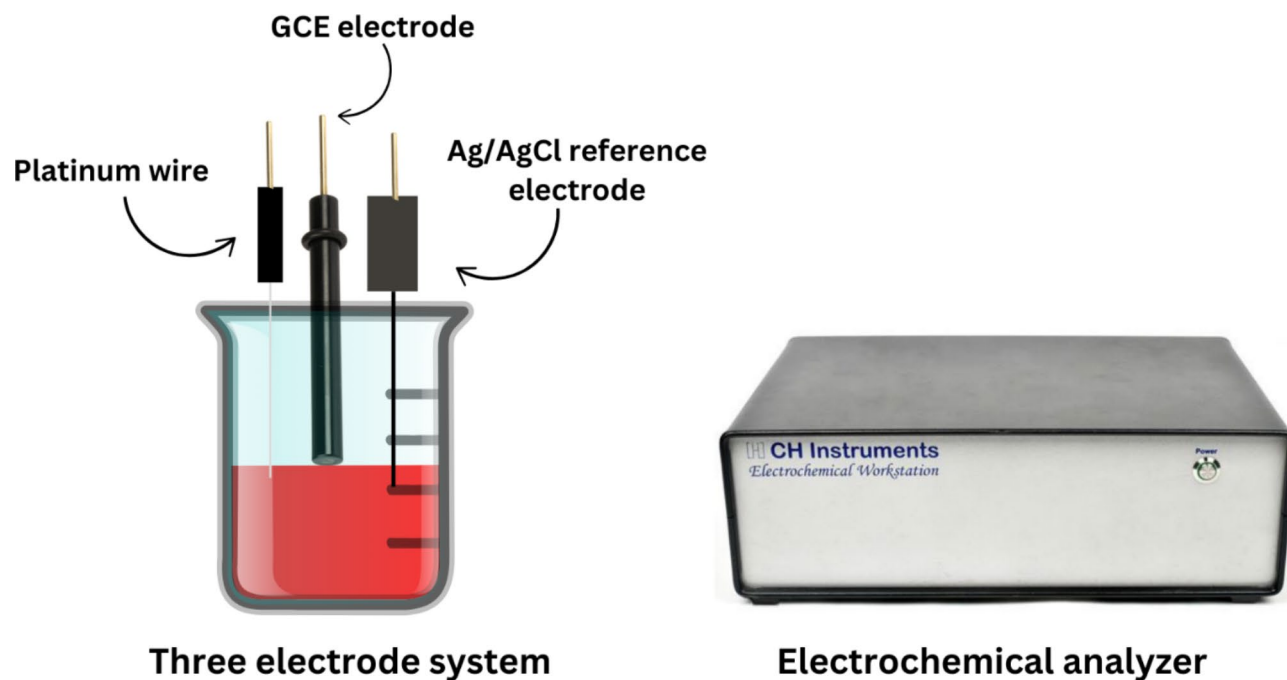
Fig. 2. Representation of three-electrode system used for the electrochemical calculation and the CHI instrument.

the COMPASS II forcefield was chosen due to its advantages of having accuracy and its compatibility with most organic as well as inorganic molecules i.e., its ability to unify force fields of two types of system[26]. The cell parameters were optimized during the geometry optimization calculation. The constructed simulation cell is presented in Fig. 3.

Geometry optimization/packing
The geometry optimization of the adsorbent, adsorbate and water molecule was performed using the forcite module with SMART algorithm and COMPASSII forcefield. For the adsorption of dye in an aqueous medium, water molecules were packed in the geometry-optimized cell of the adsorbent using the amorphous cell module, the density of the system was kept at 2.300 g/cc, with COMPASSII forcefield. The details of the set parameters and functionals used for calculations are mentioned in Table 1.

Adsorption calculation
The adsorption of dye on the adsorbent surface was studied using the adsorption locator module of the Biovia Materials Studio 2020. The adsorption locator module utilizes the Monte Carlo calculations to find out the most stable configuration of the adsorbate over the adsorbent surface. The simulated annealing runs a set number of cycles of hot and cold temperatures to find out the optimal interaction in that range[27]. The adsorption energies of dye adsorption over the surface were analysed in vacuum as well as in the presence of water. The simulation details are mentioned in Table 1.

Molecular dynamics (MD) simulation
MD simulation of the best-adsorbed system was performed on its optimal adsorption geometry in the presence of water molecules to study the adsorbate-adsorbent interaction energies in the dynamic system[28]. The density of the simulation box was 2.310 g/cm^3, which was generated using the amorphous cell packing module. The Forcite module of the materials studio was used to perform the dynamics in the NVT ensemble, the temperature was fixed at 298 K, Nose method was used for temperature control along with geometry optimization using the smart algorithm. To calculate electrostatic and Van der Waals interactions atom-based simulation methodologies were utilized. The simulation details are mentioned in Table 1.

Adsorption experiments
Adsorption experiments were carried out to investigate the adsorption of CR on the surface of adsorbents i.e., ZnO, Co-doped ZnO, La-doped ZnO and Ce-doped ZnO, respectively. The influence of adsorbent dose (80 mg), contact time (30, 60, 90, 120, 150 and 180 min, respectively), and initial dye concentration (10 mg/L) at room temperature were evaluated in this work. The reaction solution having 80 mg adsorbent/ 80 mL dye solution was kept for constant stirring in a completely dark environment and after every 30 min the change in colour of the solution was observed.
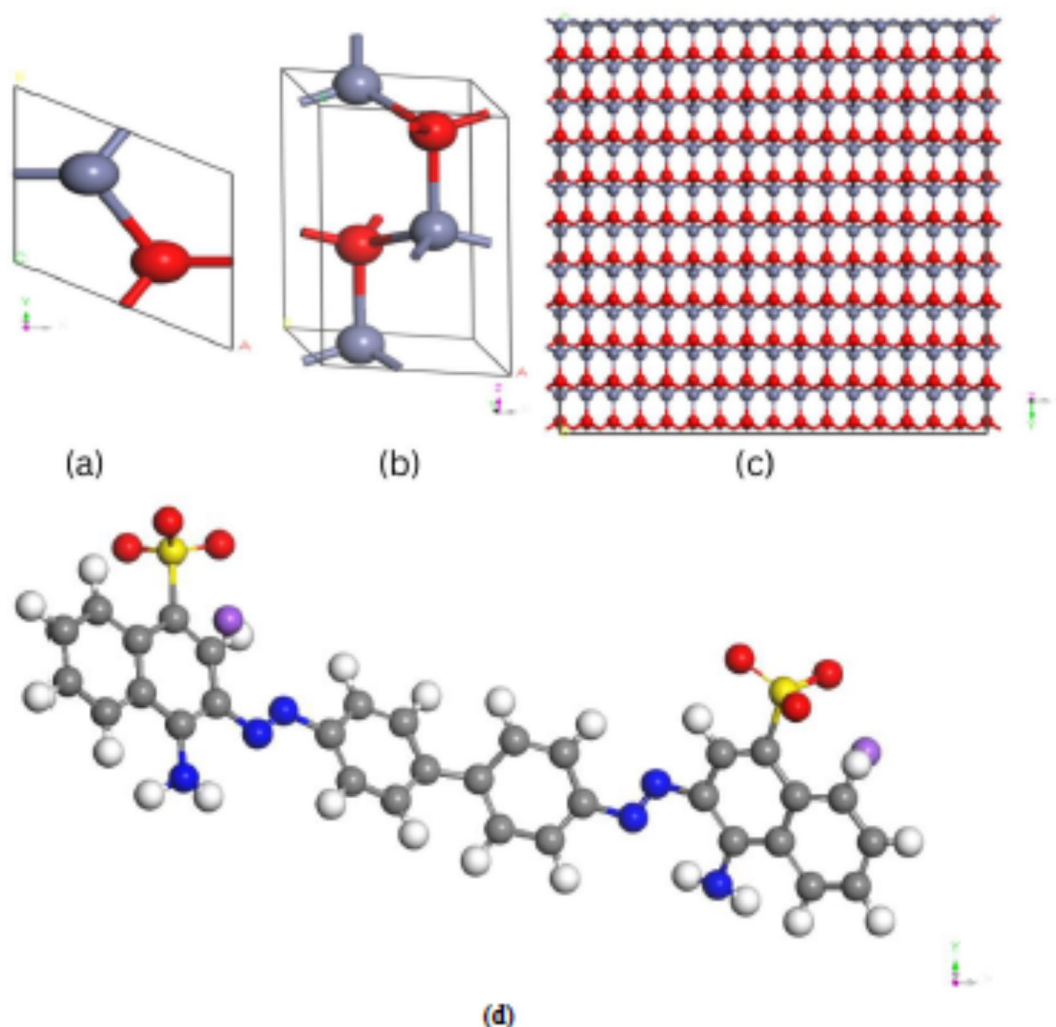
Fig. 3. (a) View onto of the ZnO unit cell (b) View across of ZnO unit cell (c) ZnO (plane 100) taken for adsorption studies (d) atomistic view of the CR molecule.

Result and discussion
X-ray diffraction patterns of the synthesized materials
The crystalline nature of the synthesized ZnO and its doped compounds was analyzed using XRD analysis and the results are depicted in Fig. 4. For ZnO compound the peaks at 2θ values of 31.71°, 34.43 °, 36.17°, 47.53°, 56.59°, 62.84°, 67.91° and 69.0° were ascribed to the (100), (002), (101), (102), (110), (103), (112) and (211) crystal planes, respectively, indicating the wurtzite structure[29]. However, there was no additional peak observed in the case of Co doping in the ZnO crystal lattice but showed the lowering of intensity. This could be attributed to the inclusion of Co ions into the ZnO lattice, resulting in the change in orientation of the ZnO lattice[30]. Another reason could be the larger ionic radius of Co (0.076 nm) compared to the Zn (0.074 nm), hence a decrease in the peak intensity would be expected[30]. Furthermore, with La and Ce doping, the peaks shifted slightly towards the lower angle. This could be due to the larger ionic radius of La (0.103 nm) and Ce (0.087 nm) as compared to Zn (0.074 nm), creating the expansion of lattice and hence peaks shifted towards the lower 2θ values. Besides, for La and Ce doped ZnO compounds small peaks at 30.18° and 28.44° were observed at (011) and (111) plane, respectively, belonging to the cubic structure of La_2O_3 and CeO_2[29,31,32].

The ionic radius of a dopant plays a crucial role in determining the crystal lattice parameters and, consequently, the XRD peak positions. Smaller dopants like Co^{2+} cause the peaks to shift to higher angles, while larger dopants like La^{3+} and Ce^{4+} cause shifts to lower angles. When a dopant ion with a different ionic radius replaces Zn^{2+} ions in the ZnO lattice, it can cause either expansion or contraction of the crystal lattice, depending on whether the dopant ion is larger or smaller than the Zn^{2+} ion. When Co^{2+} substitutes for Zn^{2+} in the ZnO lattice, the slight reduction in ionic size can cause a minor contraction of the lattice. This contraction typically results in a shift of the XRD peaks to slightly higher 2θ values due to the decrease in lattice spacing. La^{3+} has a significantly larger ionic radius compared to Zn^{2+}. When La^{3+} ions are incorporated into the ZnO lattice, they cause an expansion of the lattice due to the larger ionic size. This expansion increases the lattice parameters, leading to a shift in the XRD peaks to lower 2θ values, as the lattice spacing increases. Ce^{4+} has an ionic radius of 0.087 nm, which is also

Module	Task	
Frocite	Geometry optimization	Dynamics
	Algorithm: Smart Quality: Fine Energy (kcal mol^{-1}): 1×10^{-4} Force (kcal mol^{-1}): 0.005 Stress (GPa): 0.005 Displacement (Å): 5×10^{-5} Max. iterations: 500 Forcefield: COMPASSII Charges: Forcefield assigned Electrostatic: Atom Based Van der Waals: Atom Based Temperature: 298.0 K Pressure: 1 bar	Ensemble: NVT Quality: Fine Initial velocities: Random Temperature: 298.15 Time step: 0.5 fs Total simulation time: 1000ps Number of steps: 2,000,000 Frame output every: 5000 steps Thermostat: Nose Q ratio: 0.01 Forcefield: COMPASSII Charges: forcefield Assigned Electrostatics: Ewald based Van der Waals: Atom based
Adsorption locator	Task: Simulated annealing Number of cycles: 5 Steps per cycle: 50,000 Automated temperature control: Yes Monte Carlo options Conformer: 1 Rotate: 1 Translate: 1 Regrow: 0.1 Quality: fine Adsorbate: CR Forcefield: COMPASSII Charges: forcefield assigned Electrostatics: atom-based Van der Waals: Atom based	
Amorphous cell	Task: Packing Quality: Fine Density: 2.3 g/cc Bias Temperature: 298 K Segment lookahead: 1 Loading steps: 1000 Optimize geometry: Yes Forcefield: COMPASSII Charges: Forcefield assigned Electrostatics: Ewald based Van der Waals: Atom based	

Table 1. Description of Jobs and modules utilized for the study of adsorption.

larger than that of Zn^{2+}. Similar to La-doping, the substitution of Zn^{2+} with Ce^{4+} leads to lattice expansion. This expansion shifts the XRD peaks to lower 2θ values, although the extent of the shift may differ depending on the exact size of the lattice distortion caused by Ce^{4+}.

Field emission scanning electron microscopy (FESEM)

The morphological features of synthesized samples were analyzed by FE-SEM and the results are depicted in Fig. 5. The FE-SEM pictures were taken at 1 µm, 5 µm, 200 nm and 500 nm scale bar for all the compounds. Figure 5(a) depicts the FE-SEM images of undoped ZnO, having predominantly hexagonal wurtzite structure[33]. The particles are non-uniformly spread with a relatively narrow size distribution and aggregated morphology. Whereas, Fig. 5(b) shows the morphological change after Co doping into ZnO. It was observed that there was an increase in the growth of the microsphere and the presence of larger particles due to the overlapping or aggregation of smaller particles[34]. Figure 5(c) depicts the FE-SEM image of La-doped ZnO, showing the increase in particle diameter as compared to the undoped ZnO. Also, deterioration of aggregated structure and formation of slightly uniformed individual spherical particles were observed. Furthermore, the agglomeration increased, as illustrated in Fig. 5(d) for Ce-doped ZnO.

Energy dispersive analysis of X-ray (EDAX)

The elemental composition of ZnO and doped ZnO compounds was investigated by EDAX and is shown in Fig. 6. The atomic percentage of Zn and O were found as 31.99 and 68.01%, respectively, confirming that the material primarily consists of Zn and O in proportions that are consistent with the expected stoichiometry of ZnO. The EDAX spectra have indicated the presence of Zn, O, Co, La and Ce in synthesized samples. No peaks related to any impurities were detected in the spectrum. The presence of Co, La and Ce with appropriate weight percentages in Zn-Co-O, Zn-La-O and Zn-Ce-O, respectively, and atomic percentage of the samples were confirmed by EDAX analysis and is tabulated in Table 2. Further, Fig. 7 represents the EDAX mapping, used to analyze the existence of the dopants, where yellow and red colour represent Zn and O distributions, respectively. Figure 7(a) shows the distribution of particles in ZnO, having a chemical composition of 43% Zn and 57% O. Figure 7(b-d) depicts the elemental analysis of dopants i.e., Co, La and Ce, respectively in ZnO crystal lattice. Figure 7(b) shows the elemental mapping image of Co-doped ZnO, having the chemical composition of 39% Zn, 55% O and 6% Co. Whereas, there was a slight decrease in La percentage i.e., 5% and O percentage i.e., 47% and increase in Zn (48%) in case of La-doped ZnO, shown in Fig. 7(c). On the other hand, the Ce percentage
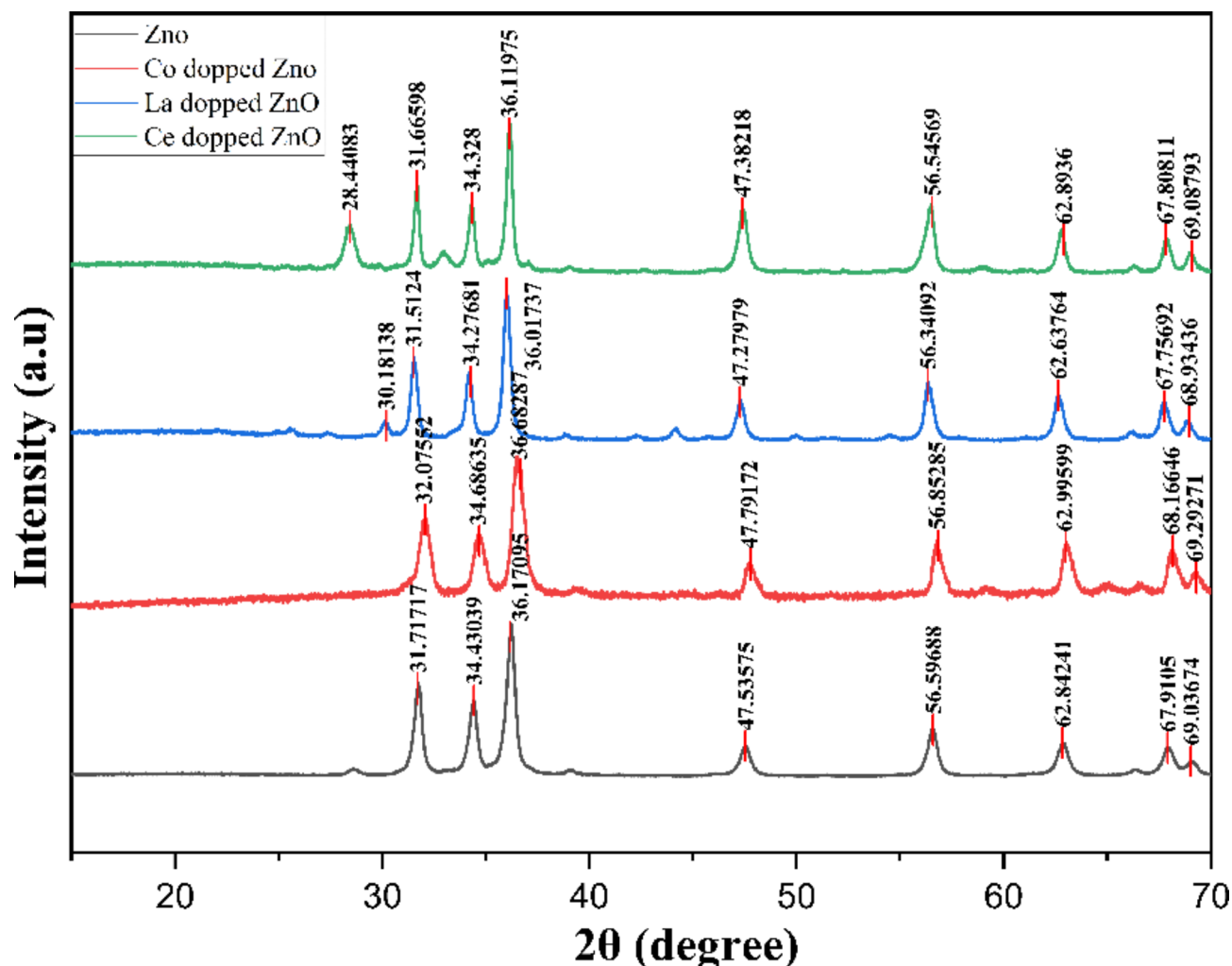
Fig. 4. XRD of (**a**) ZnO, (**b**) Co-doped, (**c**) La-doped, and (**d**) Ce-doped ZnO.

decreased to 3% along with Zn i.e., 29% for Ce-doped ZnO and the O percentage increased to 68% (Fig. 7(d)). Also, the percentage of the chemical composition of ZnO and the change in chemical composition after the addition of dopants is tabulated in Table 3.

Electrochemical investigation of adsorption of CR

Cyclic voltammetry

Cyclic voltammetry (CV) is an extensively used electrochemical method for investigating the reduction-oxidation (redox) characteristics of chemical substances. The process entails systematically varying the voltage applied to a working electrode repetitively, while simultaneously measuring the resulting electric current[35,36]. The CV curve displays the relationship between current and potential. The peaks observed in the voltammogram are indicative of the oxidation and reduction reactions of the analyte[37,38]. Figure 8 represents the CR sensing using the ZnO, Co-doped ZnO, La-doped ZnO, and Ce-doped ZnO modified GCE. Figure 8(a) shows CR sensing using a ZnO-modified electrode and a curve without the presence of CR. There was an oxidation peak at 0.32 V with a peak current of 1.20×10^{-5} A which was absent in water. This showed that it was the distinctive peak for CR oxidation. Figure 8(b) shows the Co-doped ZnO-modified electrode CV curve with and without CR. The oxidation peak for CR was at 0.32 V with a peak current of 2.39×10^{-6} A. Figure 8(c) represents the CV for blank and CR using a La-doped ZnO-modified electrode. An oxidative peak at 0.30 V with a peak current of 5.92×10^{-6} A was observed for CR sensing. For Ce-doped ZnO (Fig. 8(d)) the oxidative peak was observed at 0.32 V with a peak current of 2.21×10^{-6} A.

Figure 9 displays CV curves that demonstrate the electrochemical characteristics of different ZnO composites: ZnO, Co-doped ZnO, La-doped ZnO, and Ce-doped ZnO. The CV measurements were conducted throughout a voltage range spanning from -1.4 V to 1.0 V. ZnO (black curve) exhibited clear redox peaks, showing its active electrochemical behaviour. When other metals were added to the ZnO composites, the CV curve changed, indicating alterations in the electrochemical characteristics of the composites. The peak current was highest for ZnO modified electrode followed by La-doped ZnO and Co-doped ZnO. The peak current was lowest for the Ce-doped ZnO-modified electrode. Figure 10 depicts the electrochemical oxidation of CR[39].
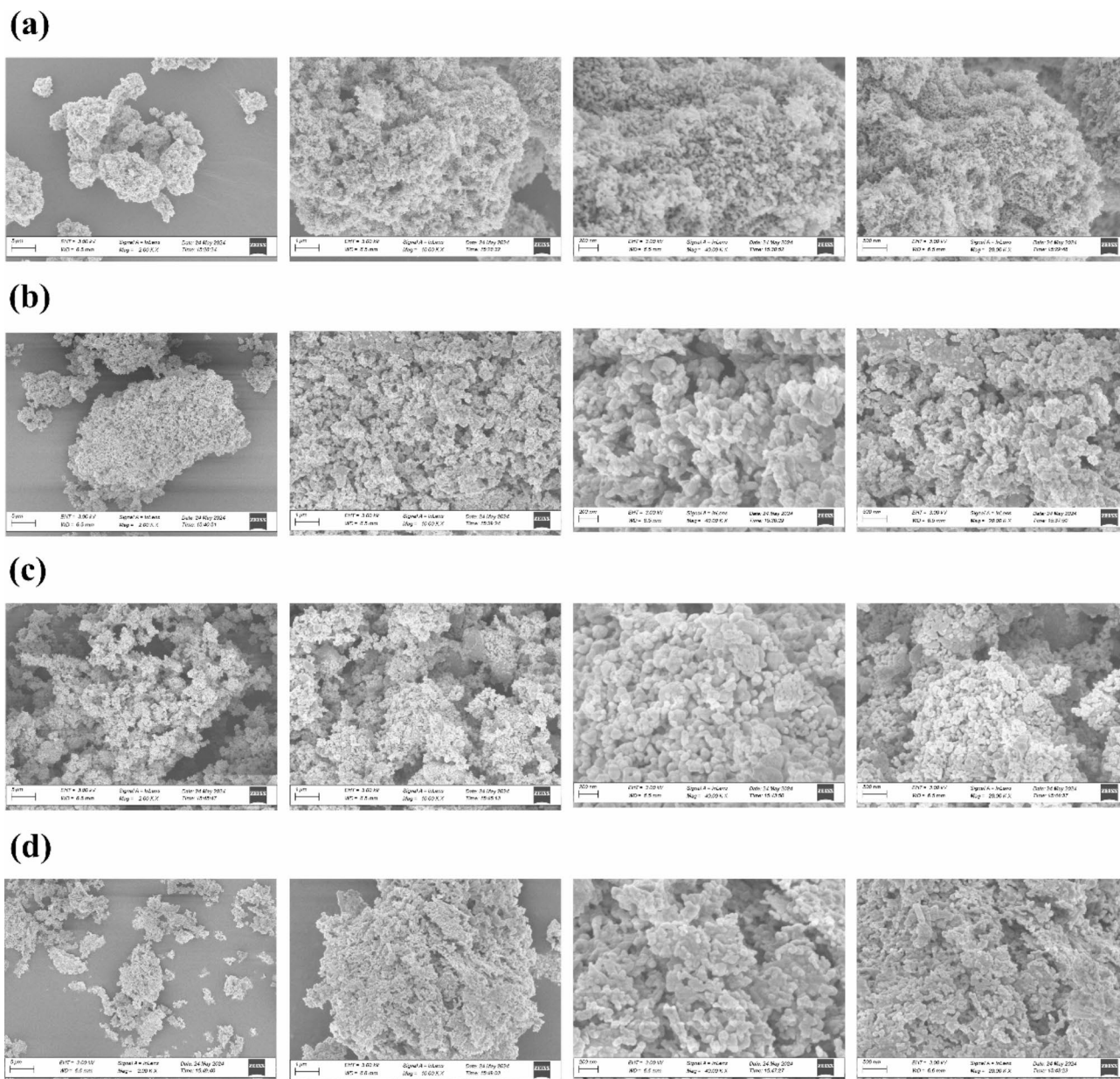
Fig. 5. FE-SEM images of (**a**) ZnO, (**b**) Co-doped, (**c**) La-doped, and (**d**) Ce-doped ZnO.

The scan rate refers to the rate at which the potential is systematically varied within the desired range. CR sensing with ZnO, Co-doped ZnO, La-doped ZnO, and Ce-doped ZnO modified GCE was done at 50 mV/s, 100 m V/s, 200 mV/s, 300 mV/s, and 400 mV/s (Fig. 11). As the scan rate was increased from 50 mV/s to 400 mV/s, both the anodic (positive current) and cathodic (negative current) peak currents experienced a rise. This behaviour is characteristic of CV and indicates that the peak currents are regulated by diffusion. As there was an increase in the peak current it was found that there was an increase in electron transfer to the electrode surface[40]. For ZnO modified electrode (Fig. 11(a)) the oxidation peak at 0.31 V with a peak current of 1.22 * 10^{-5} at scan rates of 50 and 100 mV/s. However, it was observed that at a higher scan rate, the oxidative peak was missing. For Co-doped ZnO (Fig. 11(b)) modified electrode peak current increased continuously as the scan rate was increased. Similar behaviour was observed for La-doped ZnO (Fig. 11(c)) and Ce-doped ZnO (Fig. 11(d)) modified electrodes.

Tafel plot
A Tafel plot is a graphical representation of potential on the y-axis and the log of current density log (i/A) on the axis, commonly employed in electrochemistry to examine the kinetics of electrode reactions (Fig. 12). The right side of the curve corresponds to the oxidative region and the left side corresponds to the reductive region[41]. Figure 12(a) displays the overpotentials for ZnO, Co-doped ZnO, La-doped ZnO, and Ce-doped ZnO, which serve as indicators of the efficacy of each material in catalysing the electrochemical reaction. Lower values for
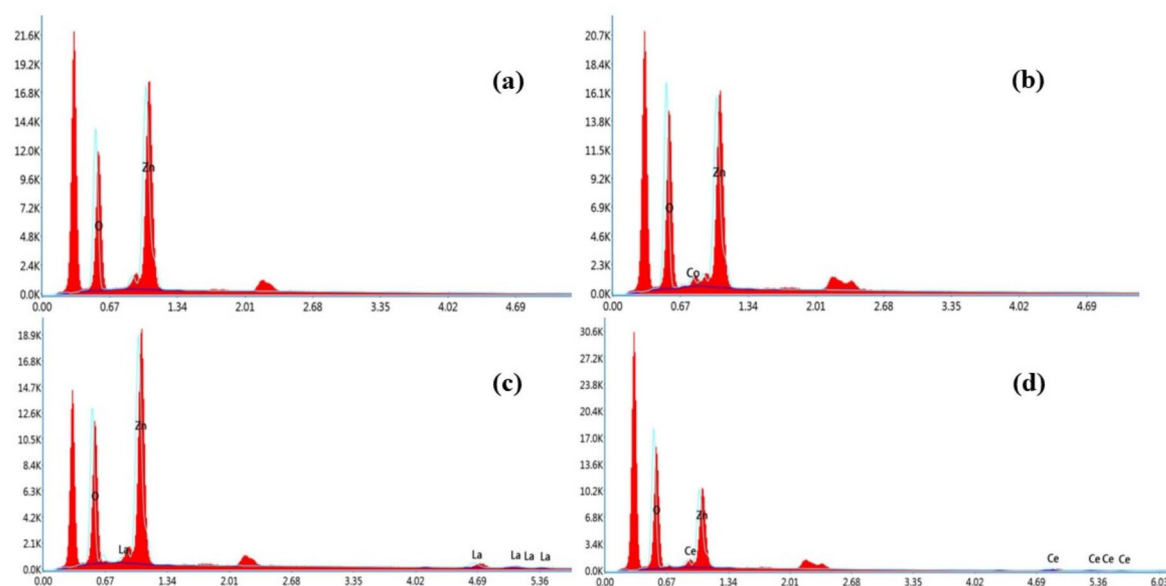
Fig. 6. EDAX of (**a**) ZnO, (**b**) Co-doped, (**c**) La-doped, and (**d**) Ce-doped ZnO.

Samples	Elements	Weight% (%)	Atomic percentage (%)
ZnO	Zn	65.78	31.99
	O	34.22	68.01
Co-doped ZnO	Zn	58.61	26.61
	O	38.89	72.13
	Co	2.50	1.26
La-doped ZnO	Zn	56.34	35.70
	O	22.39	57.96
	La	21.27	6.34
Ce-doped ZnO	Zn	41.38	20.36
	O	37.16	74.71
	Ce	21.46	4.93

Table 2. The weight% and atomic percentage of ZnO and its doped compounds.

overpotentials indicate superior catalytic efficiency[42]. The potential value for Co-doped ZnO modified was the highest which is 0.43 V and it is followed by ZnO (0.54 V) > La-doped ZnO (0.59 V) > Ce-doped ZnO (0.62 V).

The Tafel slopes, which offer valuable information about the reaction kinetics, can be determined by analysing the slopes of the linear sections in the Tafel plots. Higher slopes typically indicate slower reaction kinetics, while lower slopes indicate faster kinetics[43]. Figure 12(b) shows the slops for ZnO-modified GCE and it was found that the oxidative region had a higher slope value of 3.55 and the reductive region had a slope value of 1.89. A lower slope of the oxidative region clearly showed that oxidation was the primary process occurring at the electrode surface.

Effect of changing pH on CV
The pH can also affect the mechanism of the electrochemical reactions, potentially leading to different reaction intermediates or altering the rate of electron transfer[44]. Figure 13 represents the CV curve of CR at pH of 4, 7 and 10 with different modified electrodes. Figure 13(a) shows the CV curve for CR detection using ZnO-modified GCE. As the pH increases from 4 to 7, there is a noticeable increase in peak current, with pH 7 showing the highest peak. However, at pH 10, the peak current decreases slightly compared to pH 7 but remains higher than at pH 4. The CV curve shows a shift in the oxidation peak potential to more positive values as the pH increases from 4 to 7 to 10. Similar to the ZnO-modified electrode, the Co-doped ZnO-modified (Fig. 13(b)) electrode exhibits the highest peak current at pH 7. This suggests that the neutral pH is again the most favourable for the
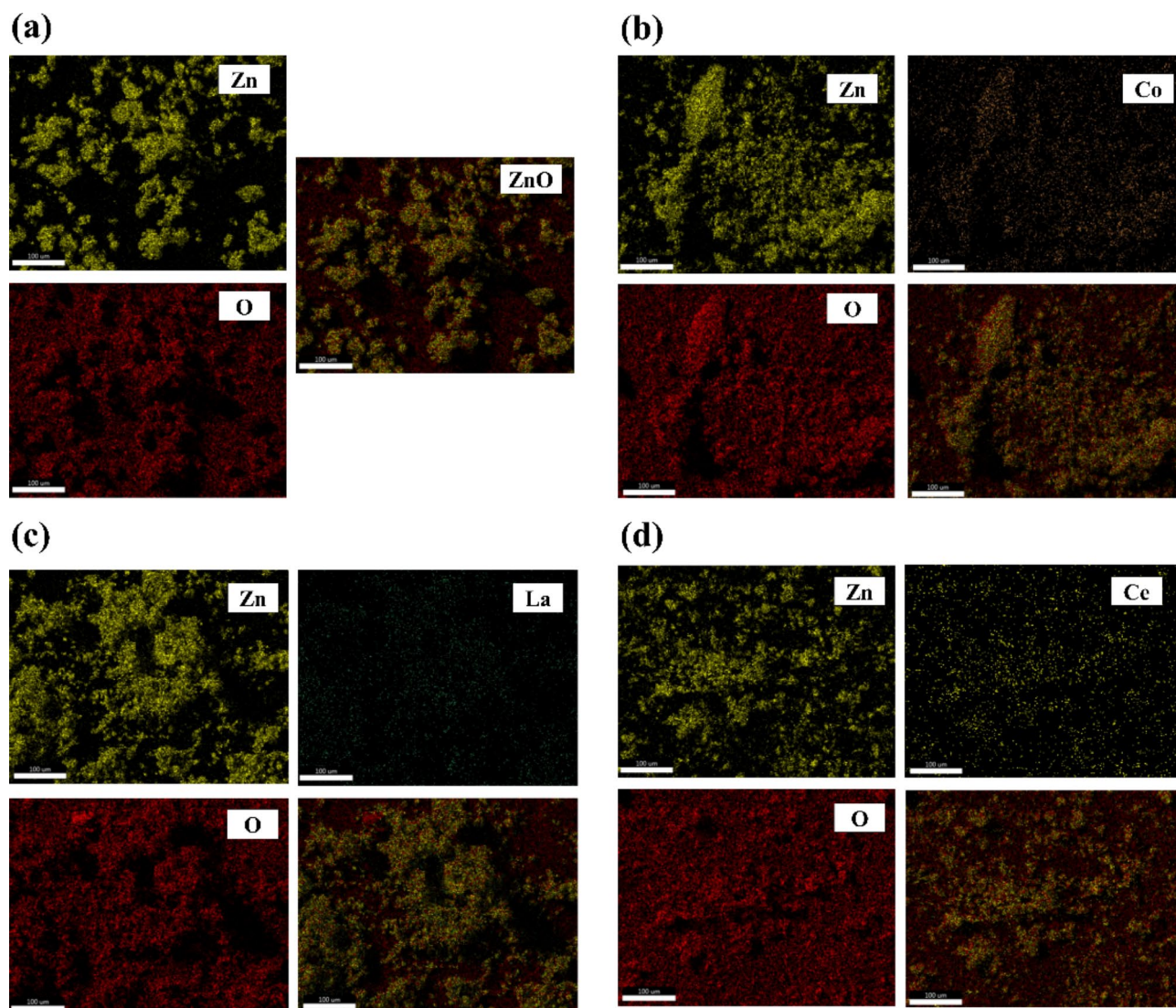
Fig. 7. EDAX mapping of (**a**) ZnO, (**b**) Co-doped, (**c**) La-doped, and (**d**) Ce-doped ZnO, respectively.

Samples	Chemical composition (%)		
	Zn	O	Dopant
ZnO	43	57	–
Co-doped ZnO	39	55	Co (6)
La-doped ZnO	48	47	La (5)
Ce-doped ZnO	29	68	Ce (3)

Table 3. Chemical composition of samples by EDAX mapping.

electrochemical activity of CR on this electrode surface. The peak currents are lower at both pH 4 and pH 10, with pH 4 showing a slightly higher current than pH 10. For the Ce-doped ZnO modified electrode (Fig. 13(c)), the current is lower at pH 4 and pH 10, with the lowest current observed at pH 4. The oxidation peaks shift to more positive potentials with increasing pH, from 4 to 7 to 10. Figure 13(d) represents the change in CV behaviour of CR with La-doped ZnO modified GCE. It was again observed that the peak current is highest at a pH of 7 and also the peak potential. The pH affects the protonation and deprotonation of CR, which in turn influences its interaction with the electrode surface. At neutral pH, the protonation state of CR is likely balanced, leading to efficient electron transfer and higher current. The surface charge of the modified electrodes varies with pH, which affects the adsorption of CR and the electron transfer process. At acidic pH, increased protonation of the
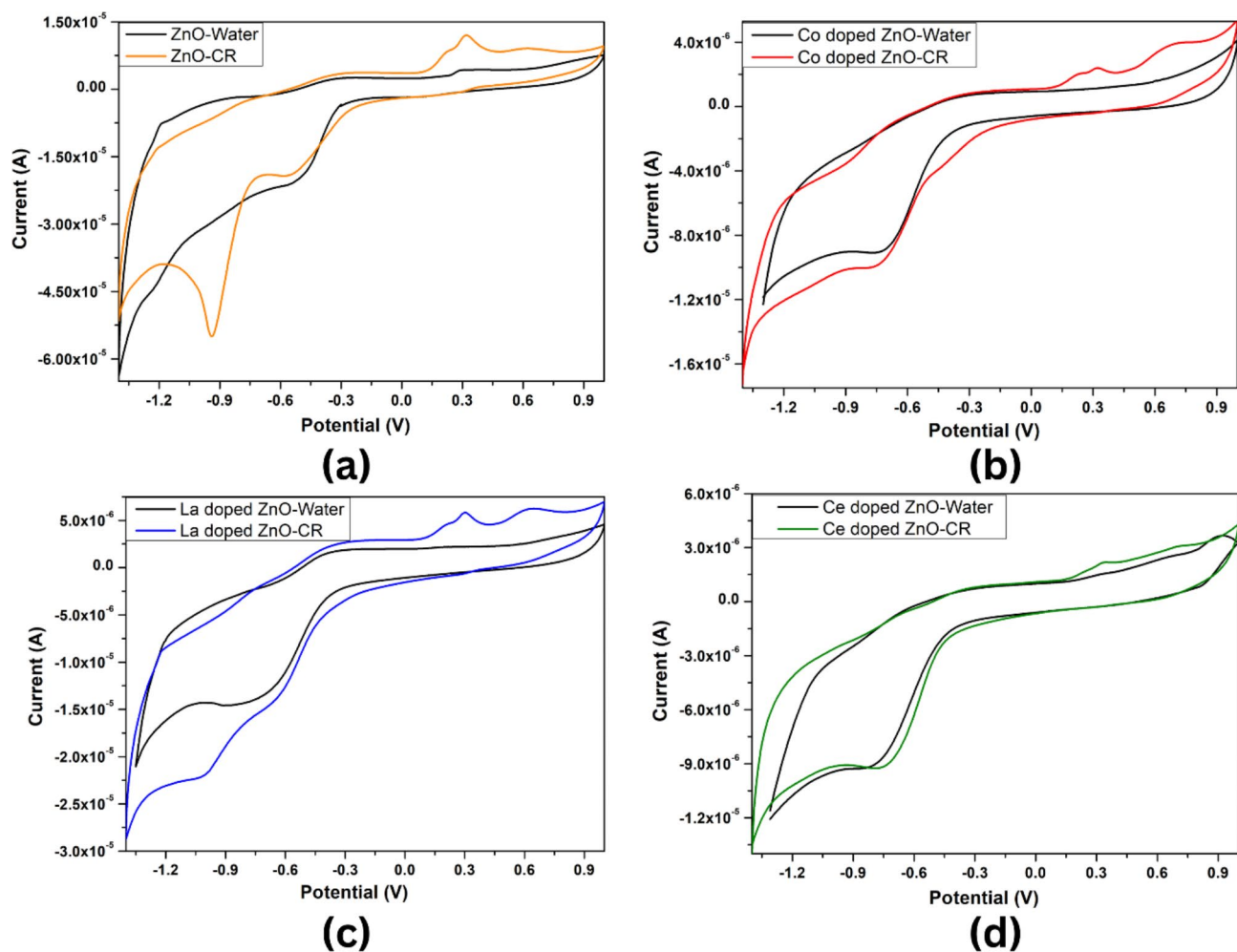
Fig. 8. CV curve for (**a**) ZnO modified GCE with water (black) and CR (orange), (**b**) Co-doped ZnO modified GCE with water (black) and CR (red), (**c**) La-doped ZnO modified GCE with water (black) and CR (blue) and, (**d**) Ce-doped ZnO modified GCE with water (black) and CR (green).
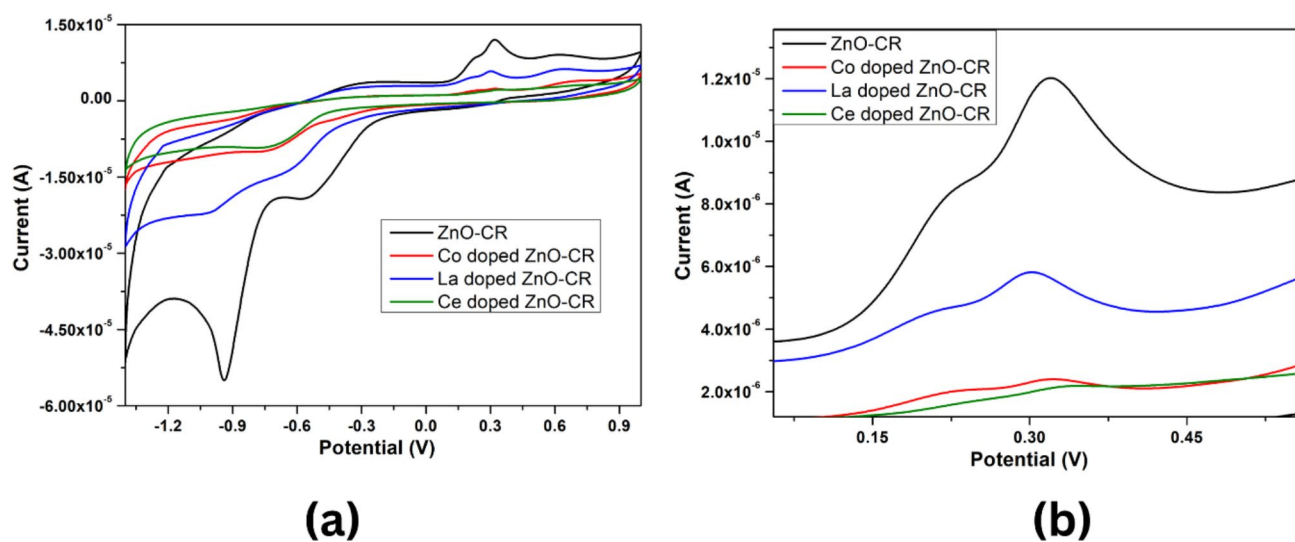

Fig. 9. CV curve for (**a**) CR with ZnO (black), Co-doped ZnO (red), La-doped ZnO (blue), and Ce-doped ZnO (green) modified GCE, (**b**) CV curve representing the oxidative peaks of CR for ZnO, Co-doped ZnO, La-doped ZnO, and Ce-doped ZnO.
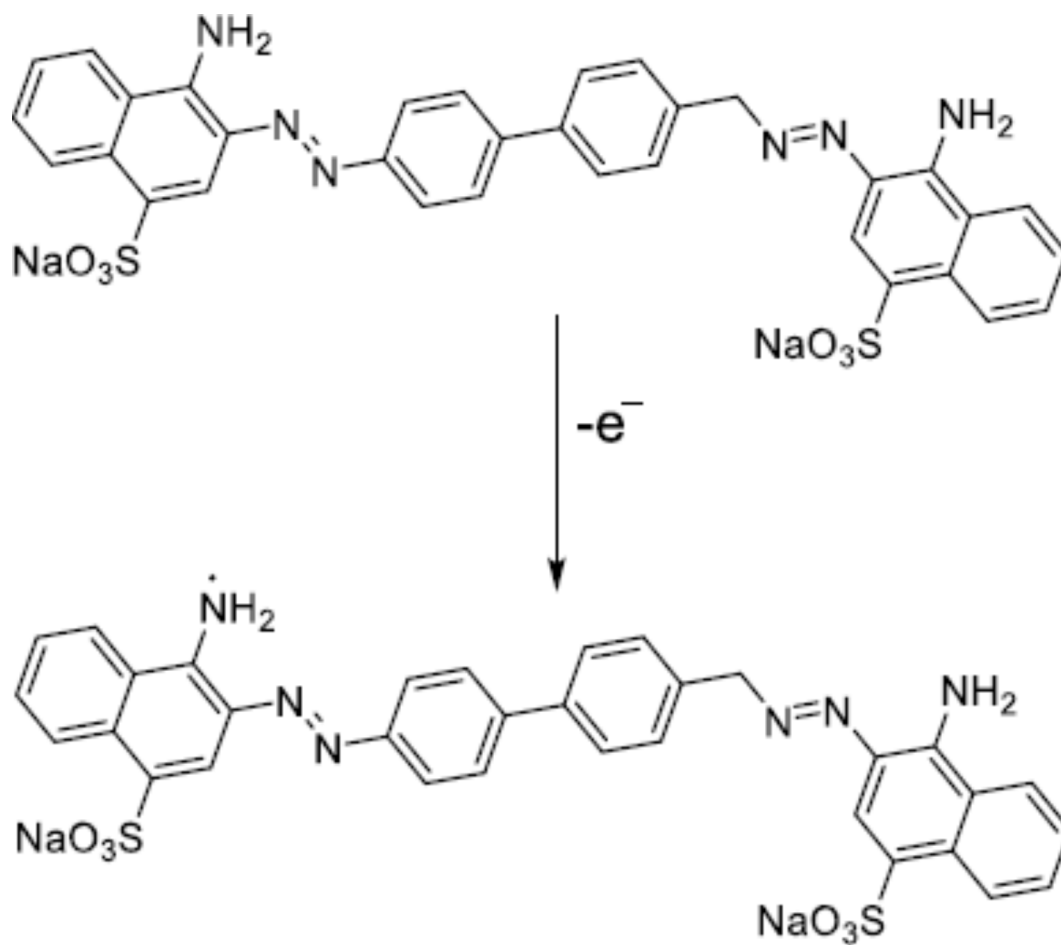
Fig. 10. Electro-oxidation mechanism of CR at GCE[39].

electrode surface may hinder the electron transfer, while at alkaline pH, the reduced availability of protons may slow down the redox reaction[45].

Computational calculations to understand the adsorption of CR

Geometry optimization
The geometries of the dye (CR) and the various adsorbent surfaces (ZnO, Co-doped ZnO, La-doped ZnO and Ce-doped ZnO) were optimized first to find out the optimal interactions between CR and the adsorbent surfaces for adsorption[46]. The COMPASSII forcefield was denoted in the potential energy surface of the atomic nuclei, on which all the molecular structures were optimized, using the Dmol3 module of Materials Studio 2020. The optimized geometries of the adsorbent surfaces and CR are presented in Fig. 14.

Adsorption calculation
The adsorption locator is a simulated annealing simulation with geometry optimization in between hot-cool cycles which is used to find out energetically most stable sites for adsorption over a broad range of materials. The module utilizes Monte Carlo calculations to find out the energetically most stable configuration of the adsorbate over the adsorbent surface, a suitable site of adsorption as well as predicts the adsorption energy[47]. For this study, simulated annealing was set to find out all the stable configurations within the energy range of 10Kcal. The most favourable orientations of the adsorption geometry are provided in Table 4. The stability of the adsorbed geometry of CR in the presence of water was compared with the adsorption of CR in vacuum. The energies of the adsorption are provided in Table 5.

The adsorption morphology of the dye in vacuum, as well as in water, gives an insight into the site preferences over the adsorbent. The distance between the CR molecule and the adsorbent sheet showed a tendency of CR to form non-covalent interactions with the adsorbent surface. In the case of ZnO, the CR molecule was adsorbed over the ZnO sheet horizontally in a bent position with one of the naphthyl units aligned horizontally while the other was aligned vertically with the sulphate unit possibly forming a non-covalent interaction with the ZnO sheet, as the distance between the sheet and the sulphate is between 3 and 4 Å. In the presence of water, the orientation of dye over the surface is inverted from that in vacuum condition, the molecule was still adsorbed in a bent position but showed higher interaction with the sheet as one of the naphthyl units along with the azo bonding laid closer to the sheet while the other naphthyl unit was pointing away from the sheet.
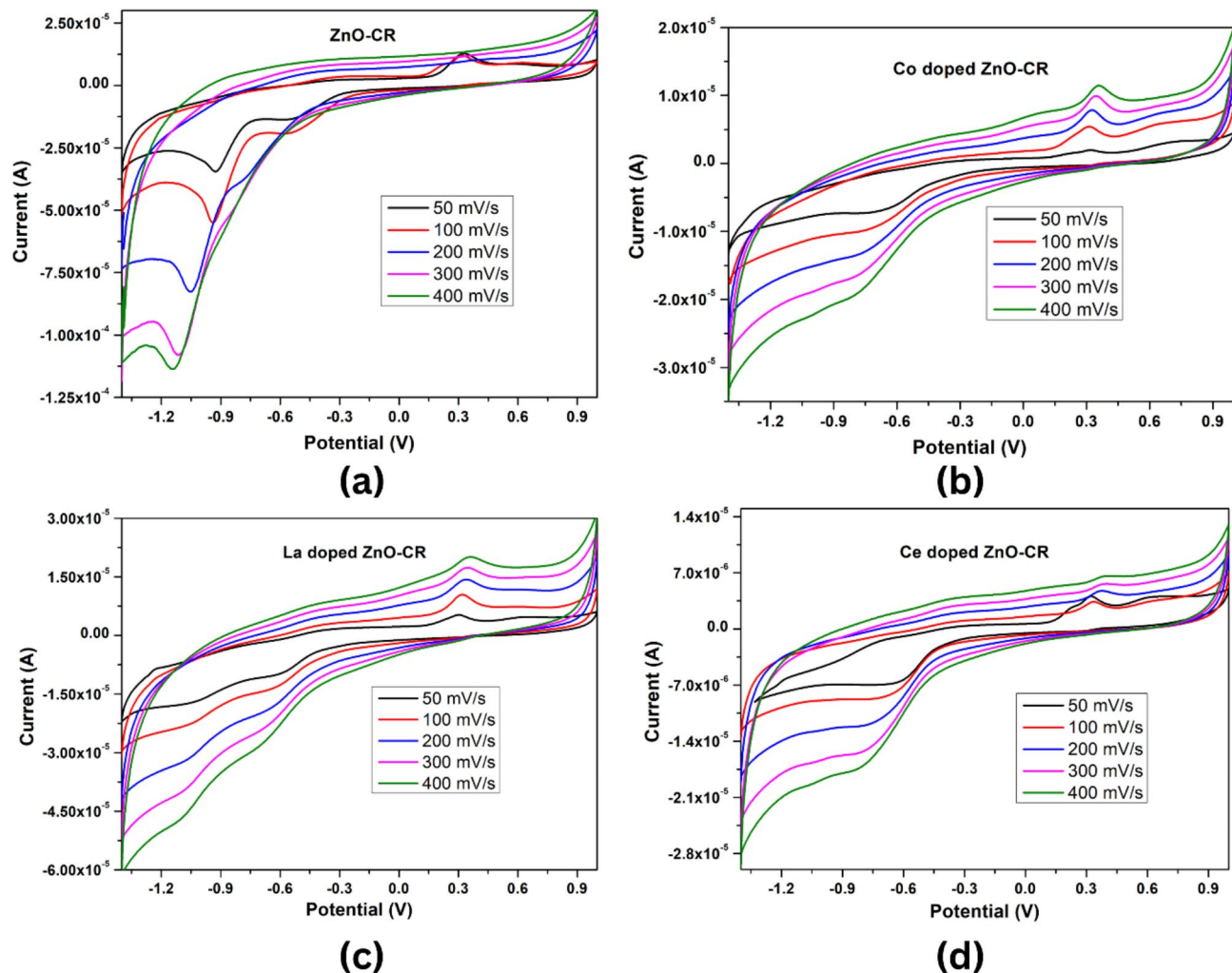
Fig. 11. Scan rate analysis for CR sensing at 50 mV/s, 100 m V/s, 200 mV/s, 300 mV/s, and 400 mV/s for, (**a**) ZnO modified electrode, (**b**) Co-doped ZnO modified electrode, (**c**) La-doped ZnO modified electrode, and (**d**) Ce-doped ZnO modified electrode.
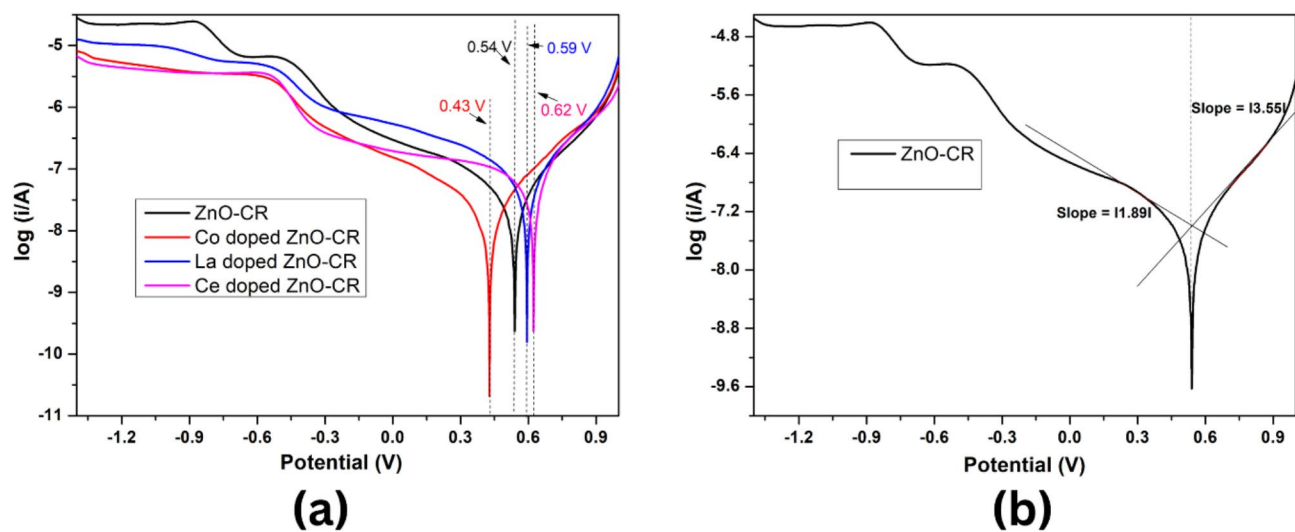

Fig. 12. Tafel plots (**a**) CR with ZnO, Co-doped ZnO, La-doped ZnO, and Ce-doped ZnO modified GCE, (**b**) Determination of slope of tafel plot for ZnO-CR.
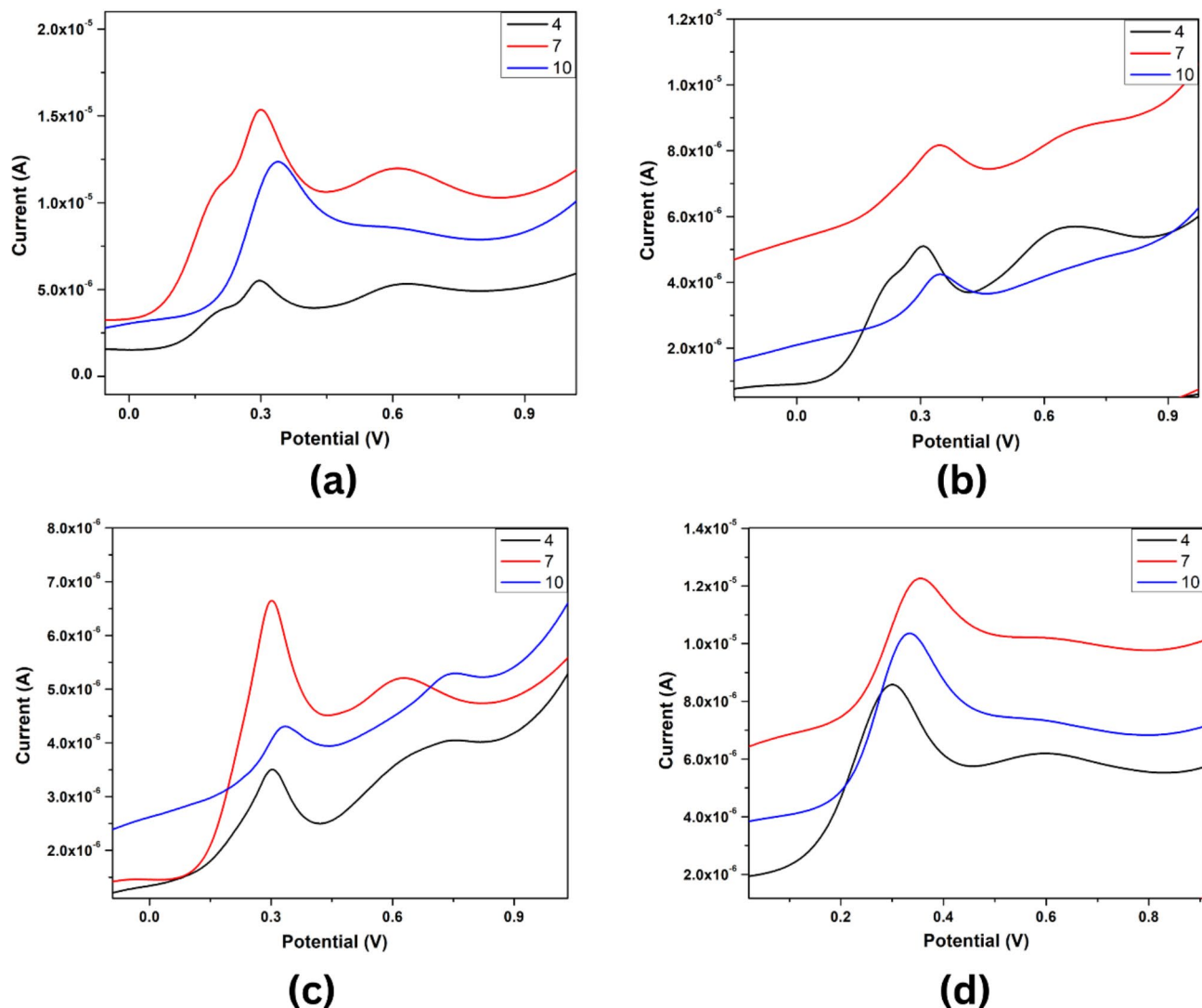
Fig. 13. CV curve of CR in PBS at different pH of 4, 7 and 10 (**a**) ZnO (**b**) Co-doped ZnO (**c**) Ce-doped ZnO (**d**) La-doped ZnO.

In Co-doped ZnO the dye molecule was adsorbed in the horizontal position with the structure of the dye bent at the biphenyl site. The bent ring lying outside the box might interact with the repeating units of the system, which requires further investigation. In an aqueous medium, the orientation of the dye molecule was bent, and positioned through the adjacent faces of the unit cell with sulphate groups pointing away from the adsorbent surface. The minimum average distance between the sheet and the amino group of the dye molecule is around 4–5Å.

In La-doped ZnO, the dye molecule lies vertically along the centre of the adsorbent sheet with both the sulphate groups interacting with the adsorbent surface with an average distance of around 3.5Å. Showing the possibility of electrostatic interaction with the adsorbent surface. In aqueous medium the orientation of the ring was half vertical while half of the molecule was aligned somewhat horizontally over the surface, the possibility of interaction was still among the sulphate groups and the sheets due to its closer proximity.

Lastly for the Ce-doped ZnO, the dye molecule is aligned vertically over the surface in a bent position in both, vacuum as well as aqueous conditions, which eliminates the possibility of charge transfer interaction. The sulphate groups of the dye were found to lie closer to the adsorbent surface indicating a possibility of electrostatic interaction. The change in both cases is the distance between the sulphate groups and the Ce-doped ZnO sheet; the dye molecule lies closer to the sheet in a vacuum than in an aqueous condition. Thus, we can conclude that the adsorption locator module helps us understand the behaviour of interaction under different conditions.

The orientation of the adsorbate gives an insight into possible interactions among adsorbent and adsorbate. However, the energies give an insight into the stability of the adsorption or simply, the tendency to show adsorption. The energies obtained from the adsorption studies include total energy, which is the sum of the adsorption, rigid adsorption, and the deformation energy. The variations in the energy of the system during the adsorption process are depicted in Fig. 15 and the variation in energies for the adsorption of CR in water during
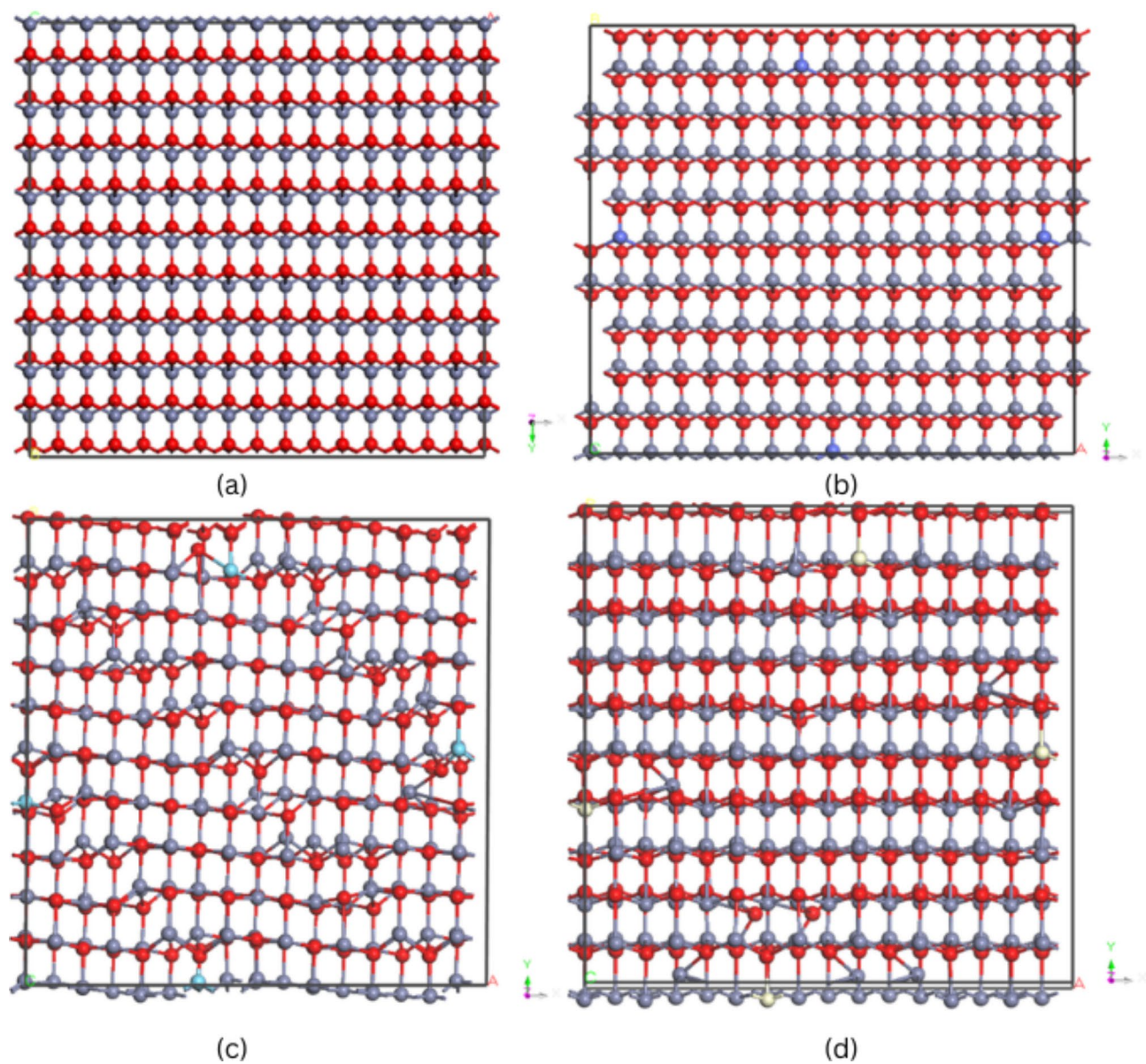
Fig. 14. Optimized geometry (onto view) of the (**a**) ZnO (**b**) Co-doped ZnO (**c**) La-doped ZnO (**d**) Ce-doped ZnO.

CR adsorption	Total energy	Adsorption energy	Rigid adsorption energy	Deformation energy	dE_{ad}/dN_i
ZnO	-1.216669×10^3	-1.638020×10^3	-1.966356×10^3	328.33591862	-1.638020×10^3
Co-doped ZnO	-1.282828×10^3	-1.704179×10^3	-1.976240×10^3	272.06049359	-1.704179×10^3
La-doped ZnO	-631.15670196	-1.052508×10^3	-1.052508×10^3	$-1.170974 \times 10^{-11}$	-1.052508×10^3
Ce-doped ZnO	-1.289853×10^3	-1.711205×10^3	-1.861619×10^3	150.41406344	-1.711205×10^3

Table 4. Adsorption energies of CR adsorption over adsorbent surfaces in vacuum.

the adsorption process is depicted in Fig. 16. Orientation of the adsorbed dye molecule over the adsorbent surface of ZnO, Co-doped ZnO, La-doped ZnO and Ce-doped ZnO in default and aqueous medium is depicted in Fig. 17. For energy calculation energy of the adsorbent surface is considered zero. The adsorption energy indicates the amount of energy released when the dye molecule gets adsorbed on the surface. The energy configurations in which the adsorbate is removed are specified by dE_{ad}/dN_i. The deformation energy indicates the relaxation energy released by the molecule when its geometry relaxes after adsorption[48]. The energies obtained

CR in Water	Total Energy	Adsorption Energy	Rigid Adsorption Energy	Deformation Energy	dE_{ad}/dN_i
ZnO	-1.117571×10^3	-1.538923×10^3	-1.751662×10^3	212.73899158	-1.538923×10^3
Co-doped ZnO	-1.623445×10^3	-2.044797×10^3	-2.428686×10^3	383.88873024	-2.044797×10^3
La-doped ZnO	-676.72702009	-1.098078×10^3	-1.098078×10^3	$-1.214175 \times 10^{-10}$	-1.098078×10^3
Ce-doped ZnO	-1.467659×10^3	-1.889010×10^3	-2.192599×10^3	303.58868569	-1.889010×10^3

Table 5. Adsorption energies of CR adsorption over adsorbent surfaces in the presence of water.
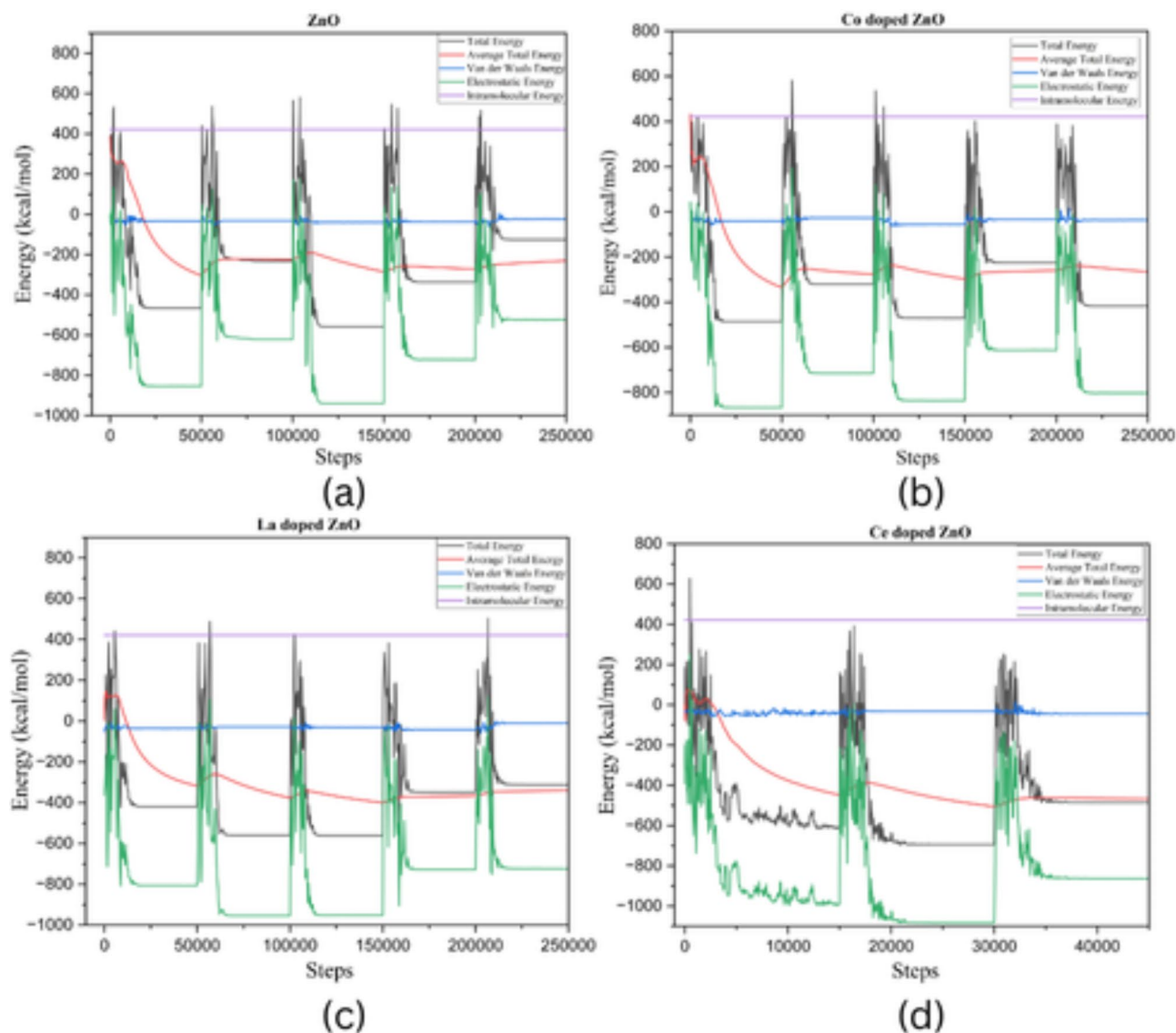
Fig. 15. Adsorption energies of (**a**) ZnO-CR, (**b**) Co-doped ZnO-CR (**c**) La-doped ZnO-CR and (**d**) Ce-doped ZnO-CR.

from the adsorption of CR over the various adsorbent surfaces in a vacuum and in the aqueous condition are depicted in Tables 4 and 5 respectively.

The higher negative value of adsorption energy indicates a more stable adsorption interaction. In vacuum, the order of adsorption energies of CR over the adsorbent surfaces was found to be Ce-doped ZnO > Co-doped ZnO > ZnO > La-doped ZnO. In the case of adsorption in aqueous condition, the order of adsorption energy was Co-doped ZnO > Ce-doped ZnO > ZnO > La-doped ZnO.
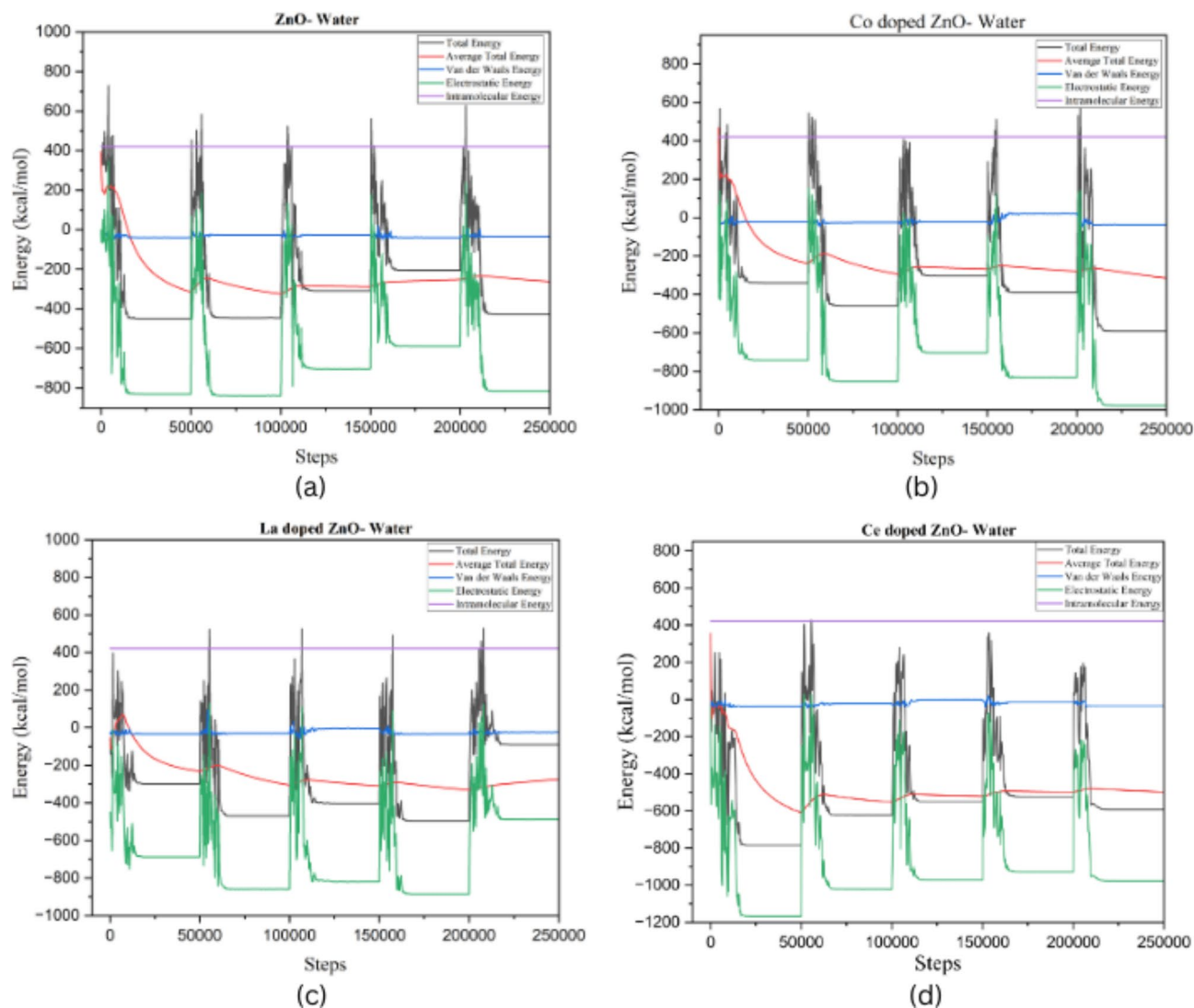
Fig. 16. Adsorption energies of (**a**) ZnO-CR, (**b**) Co-doped ZnO-CR, (**c**) La-doped ZnO-CR and (**d**) Ce doped ZnO-CR in water.

Molecular Dynamics simulations

Molecular dynamics gives an insight into the dynamics and interactions during the adsorption process. The forcefield COMPASSII was utilized to for the MD simulation calculations. The MD simulation was performed for the adsorption of CR over the Co-doped ZnO since it had the highest negative adsorption energy in an aqueous medium. The amorphous cell module was used to pack water molecules in the simulation cell. The Forcite module utilized for MD simulation searches for possible interactions among the dye and adsorbent surfaces within the simulation box, along with optimizing the whole arrangement. The dynamics were run using the NVT ensemble at 298 K, 308 K and 318 K for 1000 ps using a Nose mass parameter thermostat with a timestep of 0.50 fs, to understand the change in interactions with the change in temperature. The potential energy, non-bonded energy as well as temperature was monitored during the MD simulation, to determine if the simulation model achieved equilibrium within the period of MD simulation. The temperature analysis initially showed fluctuations, a steady state temperature of 298 K, 308 K and 318 K respectively, was observed within the period of 1000 ps. The energy analysis showed the system achieved stable energetics indicating attainment of equilibrium by the system. The graphs for temperature dynamics and energy dynamics are presented in Fig. 18. The total energy of the system after the MD simulation was stabilized from -238403.068 kcal/mol to -324415.476 kcal/mol at 298 K, from -238384.289 kcal/mol to -316254.173 kcal/mol at 308 K and -238365.510 kcal/mol to -317670.024 kcal/mol at 318 K. This decrease in the total energy indicates stable adsorption of dye molecule even at elevated temperature. This confirms Co-doped ZnO as a prominent candidate as an adsorbent for dye removal from wastewater. The orientation of the stabilized dye-substrate system after the MD is presented in Fig. 19.
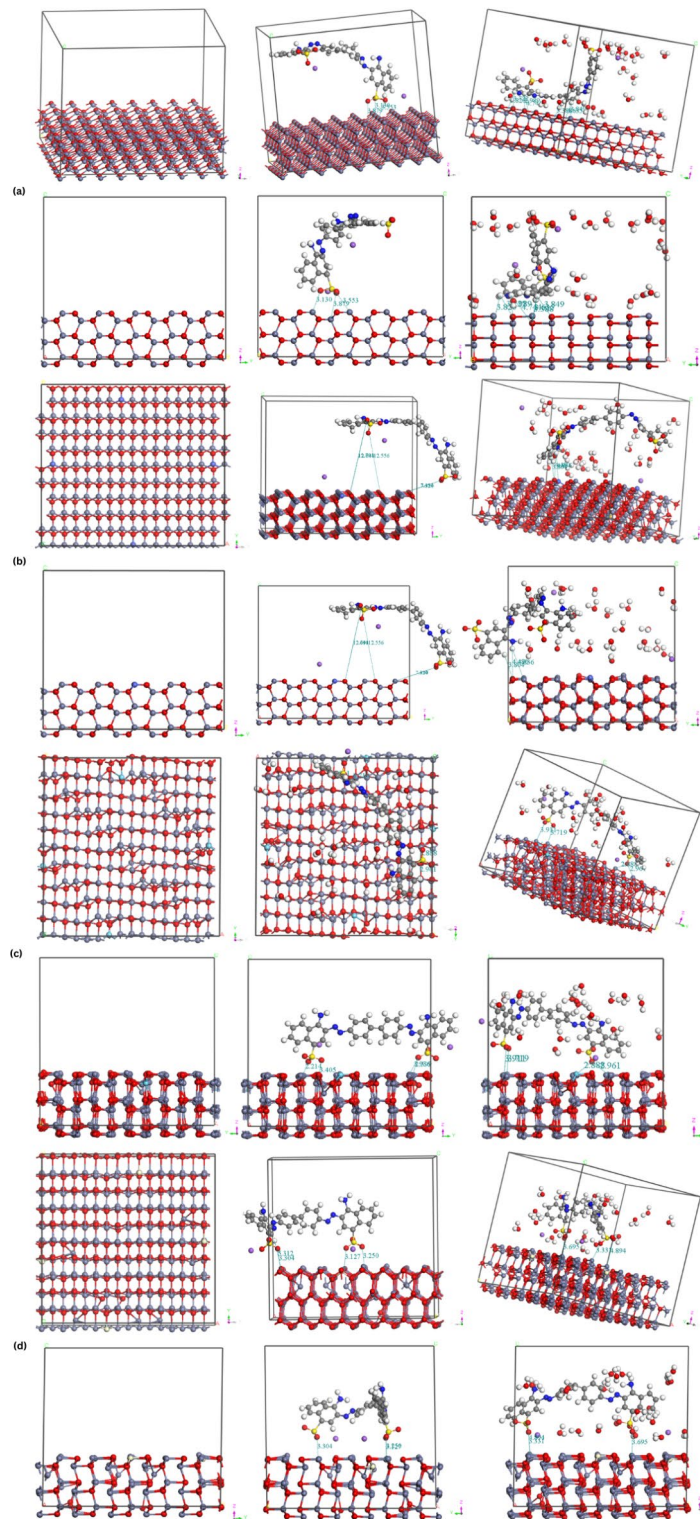
Fig. 17. Orientation of the adsorbed dye molecule over the adsorbent surface (**a**) ZnO (**b**) Co-doped ZnO (**c**) La-doped ZnO and (**d**) Ce-doped ZnO surfaces and in aqueous medium.

Adsorption of CR using ZnO-based materials

The adsorption behaviour of ZnO, Co-doped ZnO, La-doped ZnO and Ce-doped ZnO was evaluated by the decolourization of CR solution. As proposed by Debnath et al. ZnO adsorbent may possess possible binding with azo groups i.e., −N = N− of CR. However, ZnO may interact with the amine group in CR as well. This may suggest that CR was easily adsorbed by the adsorbents[49]. After every 30-minute interval time, the colour change in the dye solution was observed. This revealed a slight decrease in the dye's colour intensity, indicating progressive
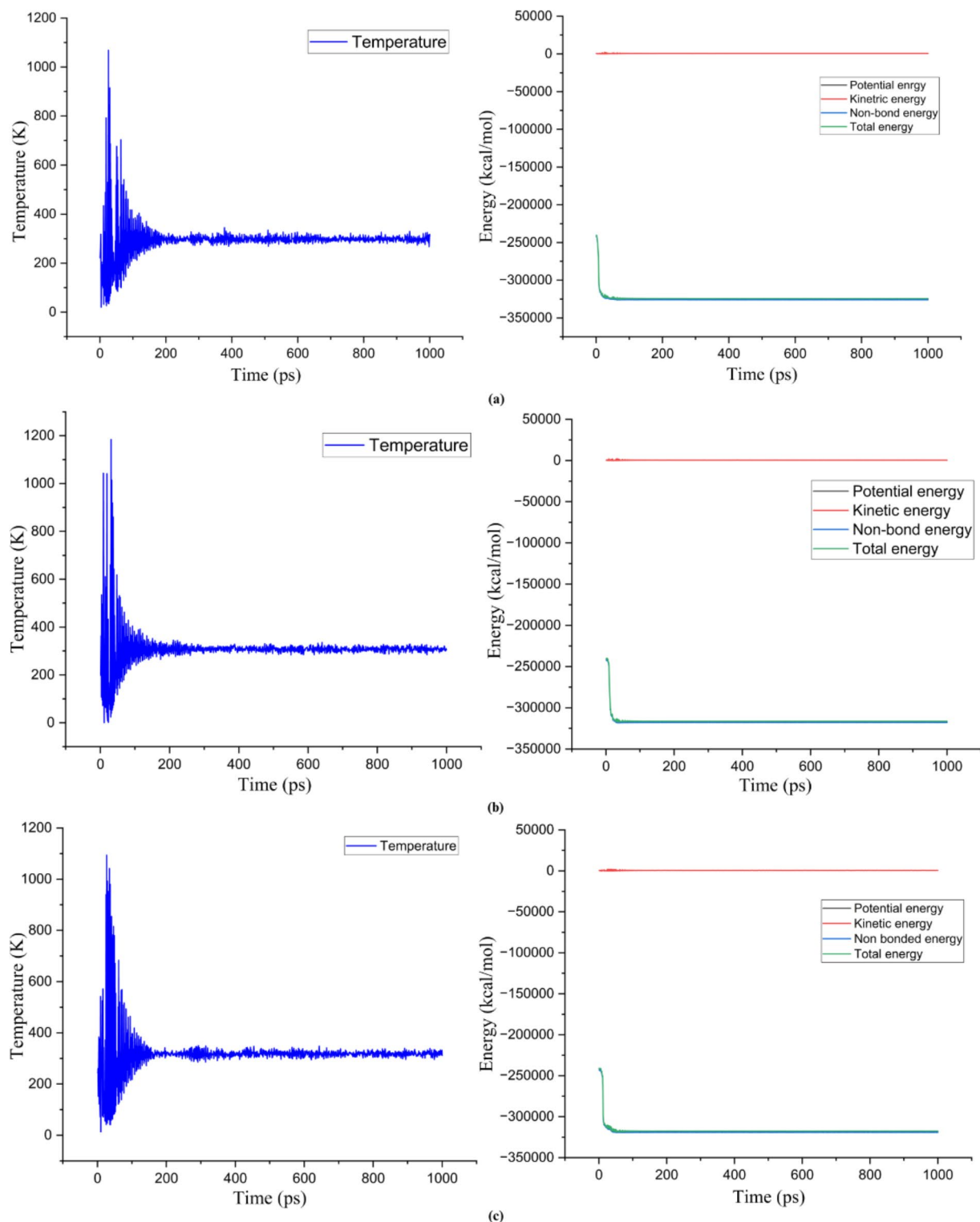
Fig. 18. Graph of Temperature dynamics and energy dynamics of the MD simulation at (**a**) 298 K, (**b**) 308 K and (**c**) 318 K.

adsorption. Remarkably, after one day, the intensity of adsorption varied with the adsorbent, the adsorption order was found to be Co-doped ZnO > ZnO > Ce-doped ZnO > La-doped ZnO. This comprehensive binding between Co-doped ZnO and CR highlights the increased potential of ZnO as a highly efficient adsorbent for dye removal in wastewater treatment applications. Figure 20 shows the adsorption of CR over different adsorbents over an interval of 30 min until 180 min and then at 24 h period.
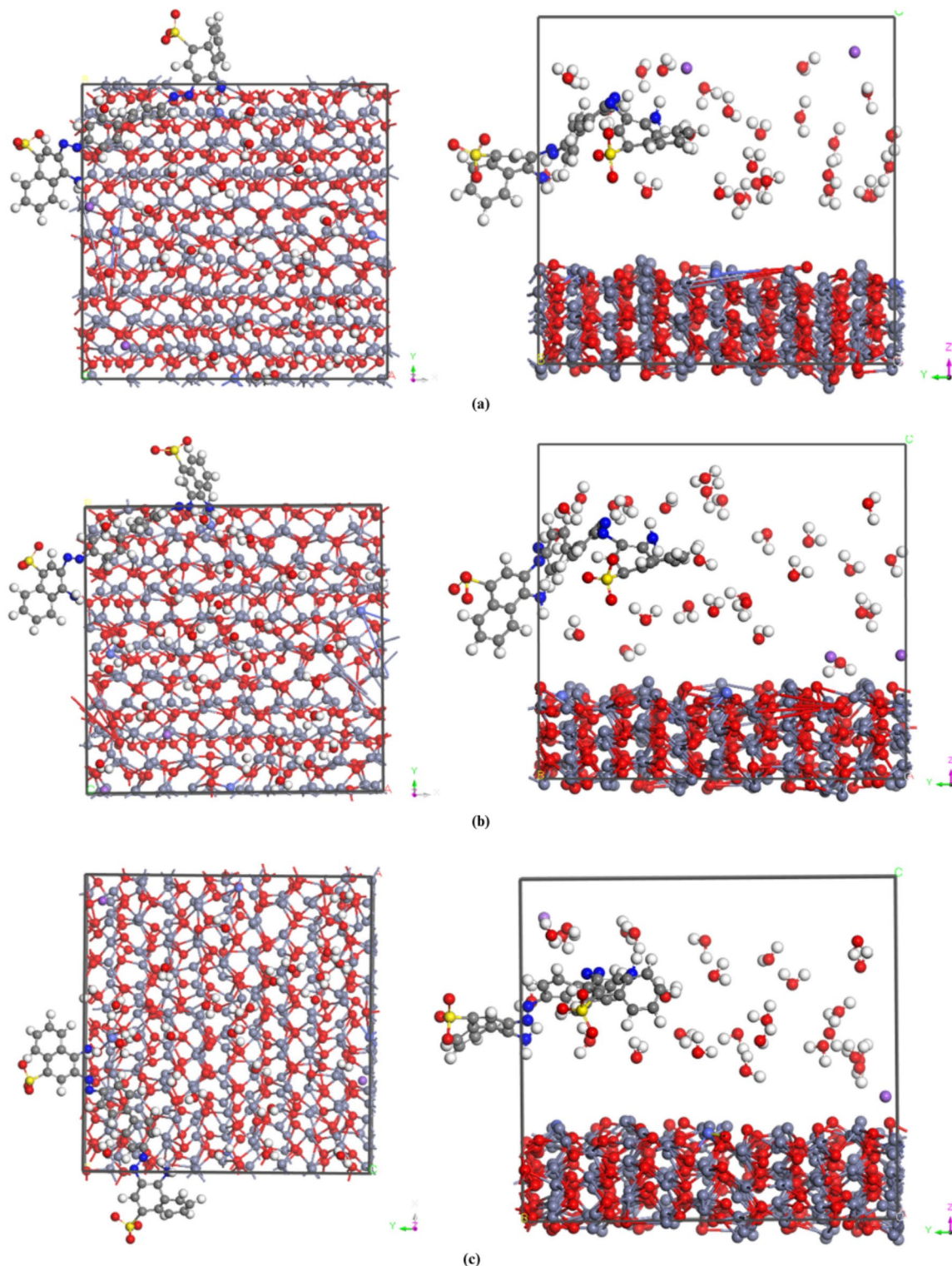
Fig. 19. Final snapshots of MD simulation of CR adsorption over Co-doped ZnO in the presence of water at (**a**) 298 K, (**b**) 308 K and (**c**) 318 K.

Experimental evidence of adsorption

To examine any change in the morphology of the adsorbent after adsorption, XRD and FTIR of the residue settled after 24 h of adsorption were performed. Figure 21 represents the XRD plot of the different adsorbents after 24 h of adsorption, the XRD pattern of adsorbents before adsorption is presented in Fig. 4.

It was observed that all samples retain the primary peaks characteristic of the hexagonal wurtzite structure of ZnO, indicating that the adsorption process did not induce a significant change in the overall crystal structure.

Fig. 20. Pictures of adsorption of CR over ZnO, Co-doped ZnO, La-doped ZnO and Ce-doped ZnO at 30 min intervals until 180 min and then at 24 h period.

However, there are noticeable variations in peak intensities compared to the before-adsorption patterns. This suggests potential changes in crystallite size or preferred orientation due to CR adsorption. Some peaks appear slightly broader in the after-adsorption patterns, which might indicate a decrease in crystallite size or increased lattice strain. Also, no additional peak was observed suggesting that no new crystalline phases were formed during the adsorption process. For ZnO, a slight decrease in peak intensities, possibly indicating a reduction in crystallite size or increased surface defects. Similar to ZnO, there is a decrease in peak intensities in Co-doped ZnO, suggesting potential changes in crystallite size or orientation. In the case of La-doped ZnO, the pattern shows a more pronounced decrease in peak intensities compared to other samples, indicating a more significant impact of CR adsorption on crystallite size or structure. In Ce-doped ZnO, the XRD pattern exhibits a relatively smaller change in peak intensities compared to the other samples, suggesting a lower degree of interaction with CR. The observed changes in peak intensities and broadening suggest that CR molecules primarily interact with the surface of the ZnO-based compounds rather than incorporating them into the crystal lattice. And, the decrease in peak intensities and potential broadening indicate a possible reduction in crystallite size due to CR adsorption. This could enhance the surface area available for adsorption. The slight peak broadening might suggest the induction of lattice strain due to the interaction between CR molecules and the adsorbent surface.
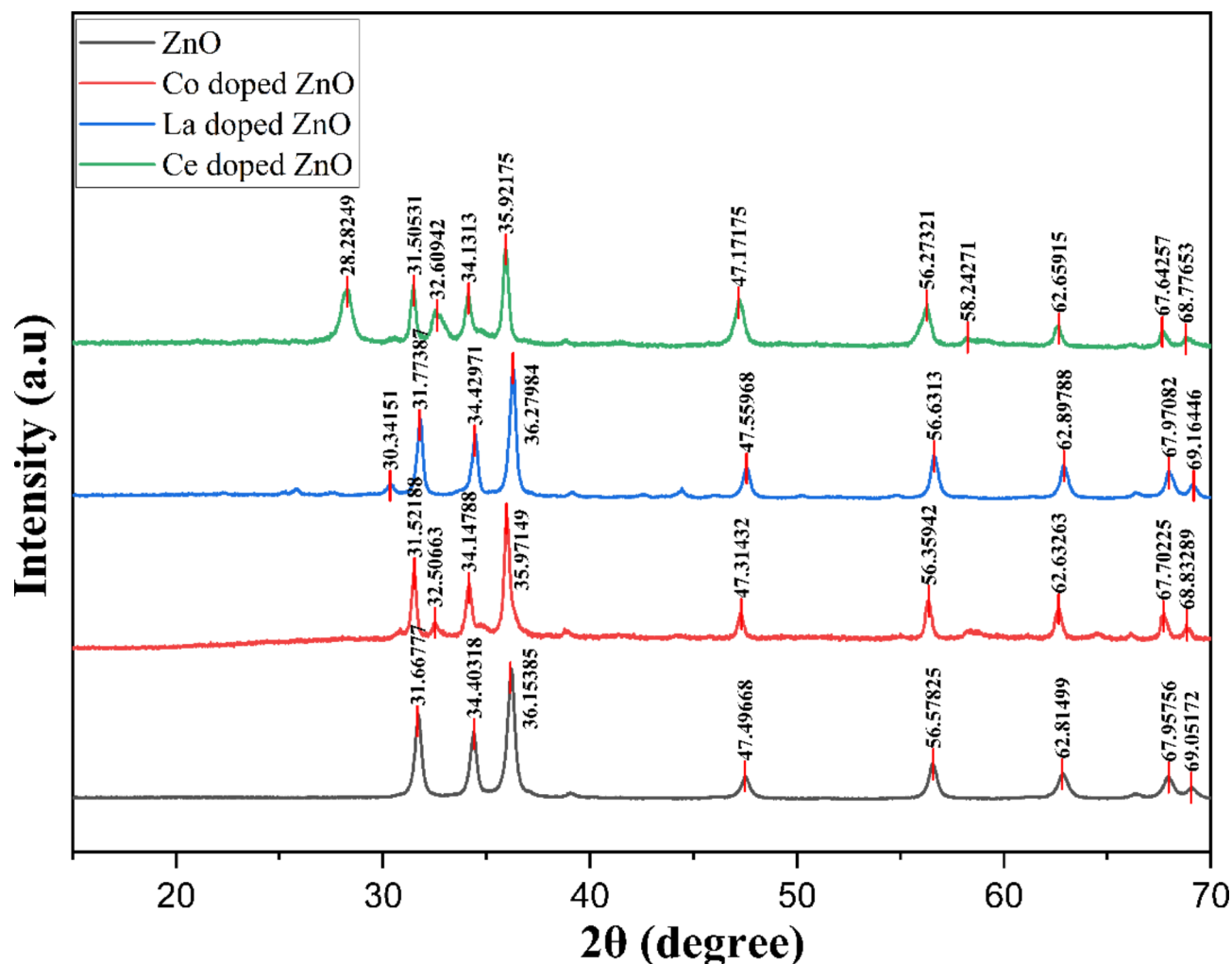
Fig. 21. The XRD pattern of adsorbent after 24 h of dye adsorption.

Figure 22 indicates the fourier-transformed infrared spectroscopy (FTIR) analysis of ZnO and doped ZnO materials before and after the adsorption of CR. The spectral pattern study suggests effective adsorption of CR molecules. In IR spectra of ZnO and doped ZnO, materials exhibited peaks ~ 3400 cm^{-1} and 2340 cm^{-1} which corresponds to the adsorbed water and CO_2 over the surface, the peak at 1386 is of asymmetric stretching of C=O while the sharp peak around 2950 cm^{-1} corresponds to the stretching vibration of CO_2[50]. The broadening or decrease in intensity of these peaks due to the effective adsorption of dye was observed to be highest in the case of Co-doped ZnO and ZnO. The multiple peaks of metal oxides were observed in the fingerprint region of low intensity[51]. The CR adsorption is also evident from the appearance of a stretching peak of the azo group (N=N) around 1590 and of S=O around 1190 cm^{-1}. The aromatic C-N stretching peak of CR was also observed near 1050 cm^{-1}[52]. In the case of La-doped ZnO very little broadening was observed indicating lower adsorption, however, changes in the fingerprinting region were observed which might suggest adsorption of CR through any specific site, thus change in the fingerprint region might suggest a change in the bonding structure of doped material due to dye. It is worth mentioning that La-doped ZnO exhibited almost no peak of adsorption of water of CO_2 over its surface as well suggesting La-doped ZnO is a weaker adsorbent. Ce-doped ZnO also exhibited only slight variation in the spectra after the adsorption of the CR molecule over its surface, only the stretching peak of the azo group (N=N) of the CR molecule was evident, suggesting some adsorption.

Conclusion

In this study, ZnO and its doped compounds (Co-doped ZnO, La-doped ZnO, and Ce-doped ZnO) were synthesized and thoroughly characterized using XRD and FE-SEM techniques. The electrochemical properties were extensively investigated through CV and Tafel plot analyses. The CV results revealed distinct oxidation peaks for CR sensing, with ZnO and its doped compounds showing varying peak currents and potentials, indicating their potential for CR detection. Specifically, the Co-doped ZnO-modified electrode exhibited the highest peak current of 2.39 × 10^{-6} A, highlighting its superior sensitivity. The Tafel plot analysis provided insight into the catalytic efficiency and reaction kinetics of the synthesized materials. Among the tested electrodes, the Co-doped ZnO demonstrated the highest potential value of 0.43 V, indicating its enhanced
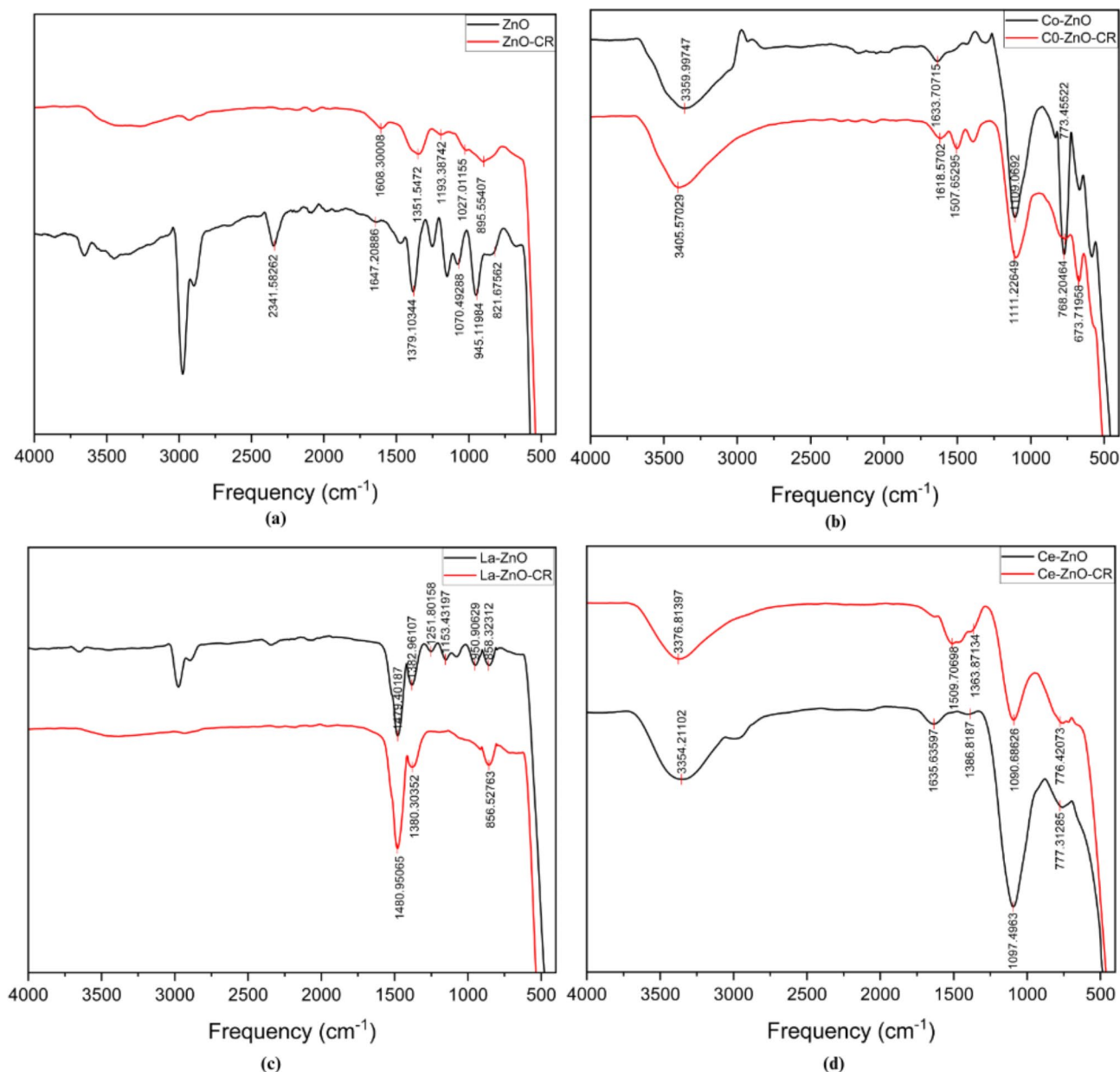
Fig. 22. FTIR spectra of (**a**) ZnO (**b**) Co-doped ZnO (**c**) La-doped ZnO and (**d**) Ce-doped ZnO before and after the adsorption of CR dye.

catalytic performance. Additionally, the analysis of Tafel slopes suggested that oxidation is the primary process at the electrode surface, with the ZnO-modified electrode showing a higher slope in the oxidative region. The quantum chemical simulation shows the favourable orientations of the dye molecule over the adsorbent surface. The higher negative values of the adsorption energies indicate successful employment of the prepared substrates for the removal of CR dye. In an aqueous medium, the order of adsorption energy was found to be Co-doped ZnO > Ce-doped ZnO > ZnO > La-doped ZnO, Co-doped ZnO showed the most favourable adsorption of the dye among the developed adsorbents. The MD simulation of Co-doped ZnO showed the system attaining a thermodynamic equilibrium within the time of 1000ps. The higher negative value of the total energy after the MD showed the stability of the system in the dynamic medium. Additionally, experimental adsorption studies revealed that after 24 h CR differentially adsorbs on the surface of adsorbents, the order of adsorption efficiency was found to be Co-doped ZnO > ZnO > Ce-doped ZnO > La-doped ZnO. Thus, we can say that Co-doped ZnO exhibited superior performance as concurred by theoretical and experimental studies. The present study not only underscores the practical utility of ZnO-doped materials in environmental remediation but also provides valuable insights for further optimization and application of ZnO-based adsorbents.

Data availability
Data will be made available from the corresponding author on reasonable request of reader.

References
1. Rápó, E. & Tonk, S. Factors affecting synthetic dye adsorption; Desorption studies: a review of results from the last five years (2017–2021). *Molecules.* **26**, 5419 (2021).
2. Hernández-Zamora, M., Martínez-Jerónimo, F. & Cristiani-Urbina, E. Cañizares-Villanueva, R. O. Congo red dye affects survival and reproduction in the cladoceran Ceriodaphnia dubia. Effects of direct and dietary exposure. *Ecotoxicology.* **25**, 1832–1840 (2016).
3. Hashemi, S. H. & Kaykhaii, M. Chapter 15 - Azo dyes: Sources, occurrence, toxicity, sampling, analysis, and their removal methods. in *Emerging Freshwater Pollutants* (eds. Dalu, T. & Tavengwa, N. T.) 267–287 (Elsevier, 2022). https://doi.org/10.1016/B978-0-12-822850-0.00013-2
4. Oladoye, P. O., Bamigboye, M. O., Ogunbiyi, O. D. & Akano, M. T. Toxicity and decontamination strategies of Congo red dye. *Groundw. Sustain. Dev.* **19**, 100844 (2022).
5. Siddiqui, S. I. et al. Investigation of Congo Red Toxicity towards different living organisms: a review. *Processes.* **11**, 807. https://doi.org/10.3390/pr11030807 (2023).
6. Sareen, D., Kaur, P. & Singh, K. Strategies in detection of metal ions using dyes. *Coord. Chem. Rev.* **265**, 125–154 (2014).
7. Bilal, M., Ihsanullah, I., Hassan Shah, M. U., Reddy, B., Aminabhavi, T. M. & A. V. & Recent advances in the removal of dyes from wastewater using low-cost adsorbents. *J. Environ. Manage.* **321**, 115981 (2022).
8. Raval, N. P., Shah, P. U. & Shah, N. K. Adsorptive amputation of hazardous azo dye Congo red from wastewater: a critical review. *Environ. Sci. Pollut. Res.* **23**, 14810–14853 (2016).
9. Dutta, S., Gupta, B., Srivastava, S. K. & Gupta, A. K. Recent advances on the removal of dyes from wastewater using various adsorbents: a critical review. *Mater. Adv.* **2**, 4497–4531 (2021).
10. Lan, D. et al. Adsorptive removal of organic dyes via porous materials for wastewater treatment in recent decades: a review on species, mechanisms and perspectives. *Chemosphere.* **293**, 133464 (2022).
11. Patil, Y., Attarde, S., Dhake, R., Fegade, U. & Alaghaz, A. M. A. Adsorption of Congo red dye using metal oxide nano-adsorbents: past, present, and future perspective. *Int. J. Chem. Kinet.* **55**, 579–605 (2023).
12. Aslam, M. et al. An understanding for the synthesis of metal NPs to Photocatalysis to Toxicity. *Plasmonics.* https://doi.org/10.1007/s11468-023-02151-x (2023).
13. Ibrahim, G. M. et al. Adsorption Mechanism Elucidation of Anionic Congo Red onto Modified magnetic nanoparticle structures by Quantum Chemical and Molecular Dynamics. *J. Mol. Struct.* **1298**, 136992 (2024).
14. Raha, S. & Ahmaruzzaman Md. ZnO nanostructured materials and their potential applications: progress, challenges and perspectives. *Nanoscale Adv.* **4**, 1868–1925 (2022).
15. Vyas, S. A. Short review on Properties and Applications of Zinc Oxide Based Thin films and devices. *Johns. Matthey Technol. Rev.* **64**, 202–218 (2020).
16. Karnchana, N., Phuruangrat, A., Thongtem, S. & Thongtem, T. Tartaric acid-assisted precipitation of visible-light-driven La-Doped ZnO Nanoparticles used for Photocatalysis of Methylene Blue. *Russ. J. Phys. Chem. A.* **96**, 1805–1816 (2022).
17. Radwan, A., Mohamed, S. O., Khalil, M. M. H. & El-Sewify, I. M. Effective adsorption of fluorescent Congo red azo dye from aqueous solution by green synthesized nanosphere ZnO/CuO composite using propolis as bee byproduct extract. *Sci. Rep.* **14**, 9061 (2024).
18. Karamipour, A. A kinetic study on Adsorption of Congo Red from Aqueous solution by ZnO- ZnFe2O4-polypyrrole magnetic nanocomposite. *Phy Chem. Res.* **4**, 291–301 (2016).
19. Sachin, S. et al. Fast and effective removal of Congo Red by Doped ZnO nanoparticles. *Nanomaterials.* **13**, 566 (2023).
20. Bello, M. O., Oyewumi-Musa, R. T., Abdus-Salam, N., Gbenro, M. T. & Egbeneye, O. G. Adsorption of Congo Red Dye from Aqueous solution using ZnO and Al2O3/ZnO composite: Isotherm, Kinetic and Thermodynamic Data. *J. Appl. Sci. Environ. Manage.* **26**, 439–447 (1970).
21. Wu, X. et al. Adsorption mechanism study of multinuclear metal coordination cluster Zn5 for anionic dyes Congo red and methyl orange: experiment and molecular simulation. *Appl. Surf. Sci.* **586**, 152745 (2022).
22. Rahali, S. et al. Adsorption Behavior of Congo Red onto Barium-Doped ZnO nanoparticles: correlation between experimental results and DFT calculations. *Langmuir.* **37**, 7285–7294 (2021).
23. Das, A. et al. Mn-Modified ZnO nanoflakes for optimal photoelectrochemical performance under visible light: experimental design and theoretical rationalization. *J. Phys. Chem. Lett.* **14**, 9604–9611 (2023).
24. Vignesh, K., Nair, A. S., Udhayakeerthana, C. & Kalaivani, T. Synthesis and characterization ZnO nanoparticles using sol-gel method and their antibacterial study. *IOP Conf. Ser. Mater. Sci. Eng.* **1219**, 012019 (2022).
25. Hasnidawani, J. N. et al. Synthesis of ZnO nanostructures using Sol-Gel Method. *Procedia Chem.* **19**, 211–216 (2016).
26. Chen, X. et al. Molecular dynamics simulation and DFT calculation of green scale and corrosion inhibitor. *Comput. Mater. Sci.* **188**, 110229 (2021).
27. Amrhar, O. et al. Computational insights into the adsorption mechanisms of anionic dyes on the rutile TiO2 (1 1 0) surface: combining SCC-DFT tight binding with quantum chemical and molecular dynamics simulations. *J. Mol. Liq.* **377**, 121554 (2023).
28. Salahshoori, I. et al. Assessing cationic dye adsorption mechanisms on MIL-53 (Al) nanostructured MOF materials using quantum chemical and molecular simulations: toward environmentally sustainable wastewater treatment. *J. Water Process. Eng.* **55**, 104081 (2023).
29. Chouchene, B. et al. High performance Ce-doped ZnO nanorods for sunlight-driven photocatalysis. *Beilstein J. Nanotechnol.* **7**, 1338–1349 (2016).
30. Abirami, N., Arulanantham, A. M. S. & Wilson, K. S. J. Structural and magnetic properties of cobalt doped ZnO thin films deposited by cost effective nebulizer spray pyrolysis technique. *Mater. Res. Express.* **7**, 026405 (2020).
31. Lu, W. & Zhu, D. Synthesis and characterization of La- and Ce-codoped polycrystal ZnO prepared by hydrothermal method for 1,2-propanediol. *Appl. Phys. A.* **125**, 68 (2019).
32. Xin, M. Crystal structure and Optical properties of ZnO:Ce Nano Film. *Molecules.* **27**, 5308 (2022).
33. Hamedani, N. F. & Farzaneh, F. Synthesis of ZnO nanocrystals with Hexagonal (Wurtzite) structure in Water using microwave irradiation. *J. Sci. Islamic Repub. Iran.* **17**, 231–234 (2006).
34. Borah, M. J., Devi, A., Borah, R. & Deka, D. Synthesis and application of Co doped ZnO as heterogeneous nanocatalyst for biodiesel production from non-edible oil. *Renew. Energy.* **133**, 512–519 (2019).
35. Navashree, N. & Parthasarathy, P. A comparative study on electrochemical behaviour of various electrolytes by cyclic voltammetry: GCE as electrode material. *Mater. Today Proc.* (2023).
36. Saha, R. & Mukhopadhyay, M. Elucidation of the decolorization of Congo Red by Trametes Versicolor laccase in presence of ABTS through cyclic voltammetry. *Enzyme Microb. Technol.* **135**, 109507 (2020).

37. Ganash, A., Alajlani, L., Ganash, E. & Al-Moubaraki, A. Efficient electrochemical degradation of Congo red dye by Pt/CuNPs electrode with its attractive performance, energy consumption, and mechanism: experimental and theoretical approaches. *J. Water Process. Eng.* **56**, 104497 (2023).
38. Yadav, S. et al. Employing Spectroscopic, Electrochemical, and in Silico Research to Investigate the Interaction of Ofloxacin. *Antibact. Drug Haemoglobin ChemistrySelect* **9**, e202400770 (2024).
39. Shetti, N. P. et al. Electrochemical detection and degradation of textile dye Congo red at graphene oxide modified electrode structure of Congo Red Dye a potential / V. *Microchem. J.* **146**, 387–392 (2019).
40. Opitz, M., Yue, J., Wallauer, J., Smarsly, B. & Roling, B. Mechanisms of Charge Storage in Nanoparticulate TiO2 and Li4Ti5O12 anodes: New insights from scan rate-dependent cyclic voltammetry. *Electrochim. Acta.* **168**, 125–132 (2015).
41. Tripathi, A. K., Priyadarshani, D., Joy, M. E., Maurya, R. & Neergat, M. The impact of overpotential on the enthalpy of activation and pre-exponential factor of electrochemical redox reactions. *Phys. Chem. Chem. Phys.* **24**, 16031–16040 (2022).
42. Liu, D. et al. Synergistic effect of an atomically dual-metal doped catalyst for highly efficient oxygen evolution. *J. Mater. Chem. Mater.* **6**, 6840–6846 (2018).
43. Antipin, D. & Risch, M. Calculation of the Tafel slope and reaction order of the oxygen evolution reaction between pH 12 and pH 14 for the adsorbate mechanism. *Electrochem. Sci. Adv.* **3**, e2100213 (2023).
44. Ganash, A., Alshammari, S. & Ganash, E. Development of a Novel Electrochemical Sensor based on Gold Nanoparticle-Modified Carbon-Paste Electrode for the Detection of Congo Red Dye. *Molecules.* **28**, 19 (2023).
45. Faizan, S., Zaid, F. & Bakhtawara & Detection and removal of Congo red via aniline-based polymer and polymer composite. *Polym. Bull.* **80**, 7971–7989 (2023).
46. Salahshoori, I. et al. Advancements in wastewater treatment: a computational analysis of adsorption characteristics of cationic dyes pollutants on amide Functionalized-MOF nanostructure MIL-53 (Al) surfaces. *Sep. Purif. Technol.* **319**, 124081 (2023).
47. Verma, C. et al. Molecular dynamics and Monte Carlo simulations as powerful tools for study of interfacial adsorption behavior of corrosion inhibitors in aqueous phase: a review. *J. Mol. Liq.* **260**, 99–120 (2018).
48. Narayanaswamy, V. et al. Adsorption of methylene blue and rhodamine b on graphene oxide-Fe3O4 nanocomposite: molecular dynamics and monte carlo simulations. *Mater. Express.* **10**, 314–324 (2020).
49. Debnath, P. & Mondal, N. K. Effective removal of Congo red dye from aqueous solution using biosynthesized zinc oxide nanoparticles. *Environ. Nanotechnol Monit. Manag.* **14**, 100320 (2020).
50. Palai, P., Muduli, S., Priyadarshini, B. & Sahoo, T. R. A facile green synthesis of ZnO nanoparticles and its adsorptive removal of Congo red dye from aqueous solution. in *Materials Today: Proceedings* 38, 2445–2451Elsevier Ltd, (2020).
51. Arul, S. & Senthilnathan, T. Preparation, characterization of mg and Al co-doped ZnO nanoparticles and its application in Congo red dye remediation. *Egypt. J. Chem.* **63**, 617–625 (2020).
52. Harja, M., Buema, G. & Bucur, D. Recent advances in removal of Congo Red dye by adsorption using an industrial waste. *Sci. Rep.* **12**, 6087 (2022).

Acknowledgements

Author contributions

Ayushi Prajapat, Mohd. Aslam, Ishika Rana, Chandrabhan Verma – Performed calculations, synthesis, analysis and draft writing; Prashant Singh, Kumar Rakesh Ranjan, Kamlesh Kumari, Akram AlFantazi – Conceptualization, Supervision and finalization of the manuscript.

Declarations

Competing interests

The authors declare no competing interests.

Additional information

Correspondence and requests for materials should be addressed to P.S., A.A. or K.K.

Reprints and permissions information is available at www.nature.com/reprints.

Publisher's note Springer Nature remains neutral with regard to jurisdictional claims in published maps and institutional affiliations.